Available online at www.sciencedirect.com

SciVerse ScienceDirect

Geochimica et Cosmochimica Acta 101 (2013) 76–95

Geochimica et Cosmochimica Acta

www.elsevier.com/locate/gca

Platinum-alloy and sulfur saturation in an arc-related basalt to rhyolite suite: Evidence from the Pual Ridge lavas, the Eastern Manus Basin

Jung-Woo Park *, Ian H. Campbell, Richard J. Arculus

Research School of Earth Sciences, The Australian National University, Canberra, ACT 0200, Australia

Received 25 January 2012; accepted in revised form 2 October 2012; Available online 13 October 2012

Abstract

We have measured the platinum group element (PGE) and Re concentrations of arc-type lavas from the Pual Ridge and the surrounding area in the Eastern Manus Basin. These magmas followed an Fe-enrichment trend to produce a wide range of compositions with MgO varying between 8 and 0.1 wt.%. We found distinct differences in the PGE geochemistry of the high (>3 wt.% MgO) and the low-Mg lavas (<3 wt.% MgO). During the early stages of fractionation, the concentrations of Pd, Cu, Au and Re increase whereas Ir, Ru, Rh and Pt decrease. Co-variations of Ir, Ru and Rh with Pt in the high-Mg lavas suggest that the depletion of these elements is due to Pt-rich alloy saturation. This is consistent with the high Pt contents in the high-Mg lavas, which is close to the solubility of Pt in the basaltic melt at similar conditions. In contrast, the concentrations of all PGE and Re drop rapidly in the low-Mg lavas (except for Ru and Ir), with the PGE concentrations falling at a rate that is appreciably faster than Cu, which we attribute to sulfide saturation. As a consequence, there is a marked decline in Pd/Cu in the low-Mg lavas and we suggest that this ratio is the best indicator of sulfide saturation in an evolving magmatic system.

A feature of the data is that duplicate analyses of the same sample often do not agree within error. We attribute this scatter to the nugget effect, with nuggets of a Pt-rich alloy in the high-Mg lavas and sulfide blebs in the low-Mg lavas. The PGE concentrations of phenocryst-bearing high-Mg lavas are higher than in the associated glassy lavas, and scatter on MgO variation diagrams is significantly reduced if only glassy lavas are considered, which indicates that the micron scale Pt-rich alloy grains are intimately associated with the phenocrysts. Our results provide strong evidence that Pt-rich alloys can crystallize from a basaltic-andesitic magma, along with the silicate minerals, and fractionate Pt from Pd during magmatic differentiation. As a consequence, Pd/Pt increases during Pt alloy fractionation and this ratio can be used to identify Pt-rich metal saturation. The Pual Ridge alloys are Pt-rich because the primary magmas are Pt-enriched and Ir-depleted, which is typical of arc-related magmas.

1. INTRODUCTION

There is an abundance of platinum group element (PGE) data for mafic and ultramafic rocks because (1) important Ni–Cu(-PGE) deposits are hosted by mafic–ultramafic rocks so there is considerable economic interests in their PGE geochemistry and (2) PGE data of these rocks provide important constraints on mantle petrogenesis, and fractional crystallization and differentiation of mantle-derived magmas. In contrast, the PGE geochemistry of felsic-intermediate rocks is virtually unknown due to scarcity of data. This is principally because the concentrations of PGE of these rocks are so low that analysis is challenging. However, many of arc-related intermediate to felsic magmatic systems are associated with hydrothermal Cu, Au and Cu–Au deposits and considered to be a primary source for the ore-forming metals (Robb, 2004). The behavior of chalcophile elements including Cu and Au will be sensitively

* Corresponding author.
E-mail address: jung.park@anu.edu.au (J.-W. Park).

0016-7037/$ - see front matter © 2012 Elsevier Ltd. All rights reserved.
http://dx.doi.org/10.1016/j.gca.2012.10.001

controlled by sulfide or volatile saturation because these elements are highly compatible with both phases. Identifying sulfide saturation in an evolving felsic-intermediate system is therefore critical to understanding the geochemistry of chalcophile elements and its potential for Cu–Au mineralization. This could be accomplished by direct analyses of these elements. However, one advantage of studying the PGE in addition to Cu and Au is that they have much higher partition coefficients with regard to immiscible sulfides than Cu and Au (Francis, 1990; Peach et al., 1990; Bezmen et al., 1994; Crocket et al., 1997; Ripley et al., 2002; Fonseca et al., 2009) and are therefore more sensitive indicators of sulfide saturation. Furthermore, the PGE are less mobile in low temperature fluids than Cu and Au (e.g. Crocket, 2000). Mobility of Cu and Au in the altered rocks associated with Cu, Au and Cu–Au mineralization often leads to erratic data that are difficult to interpret.

With these overall aims in mind, and as a first step towards understanding the geochemistry of the PGE in felsic-intermediate systems, we analyzed a suite of arc-type lavas from the Pual Ridge and vicinity that underwent extreme fractionation from basalt to rhyolite. This suite was chosen because its major and trace element geochemistry had previously been well documented by Kamenetsky et al. (2001), Moss et al. (2001), Sun et al. (2007), Jenner et al. (2010) and Park et al. (2010) who showed that it followed an Fe-enrichment trend to produce a range of compositions with MgO varying between 12 wt.% to 0.1 wt.%, and SiO_2 between 51 wt.% and 75 wt.%. Jenner et al. (2010) showed that the evolving suite becomes magnetite-saturated at 4 wt.% MgO, which lowered Fe^{3+}/Fe^{2+} of the melt, consequently the fO_2, leading to sulfide saturation at 3 wt.% MgO. We will show that the most primitive samples analyzed in this study were saturated with a Pt-rich alloy and that fractionation of this alloy depleted all of the PGE except Pd whose concentration increased with fractionation. We will also show that the rate of depletion of all PGE, including Pd, accelerated markedly once the magma reached sulfide saturation at 3 wt.% MgO.

2. GEOLOGICAL BACKGROUND AND SAMPLES

The Pual Ridge is a recent volcanic complex located in the western part of the South East Rift, Eastern Manus Basin, southwest Pacific (Fig. 1; Taylor et al., 1994; Martinez and Taylor, 1996). The Pual Ridge lavas show typical features of island arc lavas such as enrichment of Pb and LILE relative to HFSE and REE, and depletion of Nb and Ti relative to adjacent elements on a chondrite-normalized trace element diagram (Sinton et al., 2003; Park et al., 2010). These features originated from the mantle below the Pual Ridge region, which is interpreted to contain an ancient subduction component (Sinton et al., 2003; Park et al., 2010). The major and trace element data as well as Sr, Nd and Pd isotopic compositions suggest that the wide range of compositions displayed by the lavas from the Pual Ridge area is mainly caused by low pressure (~1 kbar) fractional crystallization and that the magma is derived from a homogeneous mantle source (Sinton et al., 2003; Sun et al., 2007; Jenner et al., 2010; Park et al., 2010).

The Pual Ridge lavas can be subdivided into two groups based on the onset of sulfide crystallization; sulfide-undersaturated high-Mg lavas with >3 wt.% MgO and sulfide-saturated low-Mg lavas with <3 wt.% MgO (Fig. 2). The early crystallizing mineral assemblage in the high-Mg lavas consists mainly of olivine, plagioclase and clinopyroxene, with minor Cr spinel that occurs as inclusions in olivine phenocrysts (Kamenetsky et al., 2001; Sinton et al., 2003). Fractional crystallization of plagioclase, clinopyroxene and magnetite controls the compositional variation in the low-Mg lavas (Kamenetsky et al., 2001; Sinton et al., 2003). The Pual Ridge lavas investigated here are the same samples that were analyzed by Moss et al. (2001), Sun et al. (2003, 2004, 2007) and Jenner et al. (2010), and the MgO, Cu, Au and Yb data were taken from their works.

3. ANALYTICAL TECHNIQUES

Glassy parts of the Pual Ridge lavas were hand-picked for analyses using a stereoscopic microscope to exclude altered portions. Two samples (MD3-p and MD101A-p) with phenocrysts (~10% modal phenocrysts) were analyzed in order to investigate the effect of phenocrysts on PGE and Re abundances. The selected lava fragments were cleaned ultrasonically in dilute HCl and Milli-Q water, dried, and powdered in an alumina mill. The alumina mill is known to contribute the lowest PGE contamination among conventional mills (e.g. Evans et al., 2003). Whole rock PGE and Re concentrations of the Pual Ridge lavas were measured using a Ni–sulfide fire assay – isotope dilution method, which is described in detail by Park et al. (2012c). Briefly, 0.45–3.1 g of sample powder was mixed with Ni, S and sodium borax powder in the ratio of sample:Ni:S:Na-borax = 10:1:0.5:10. A mixed enriched PGE (^{99}Ru, ^{105}Pd, ^{185}Re, ^{191}Ir, and ^{195}Pt) spike solution was added to the powder. The mixture was dried for 60 min at 100 °C and fused in a preheated furnace at 1100 °C for 30 min. In order to provide reducing conditions during fusion, a second outside crucible, containing ~0.1 g of flour was used and N_2 gas was introduced into the open furnace at a flow rate of ~0.03 m^3/min. After quenching, Ni–sulfide beads were collected and dissolved in 6M HCl. The solution was then filtered through a filter paper (0.45 μm cellulose membrane, Millipore), prior to digestion of the filter paper in aqua regia. After complete digestion, the solutions were dried down to approximately ~100 μl and diluted with 2% HNO_3.

An Agilent 7500 quadrupole ICP-MS at the Australian National University (ANU) was used to measure the isotopes of PGE and Re. All samples were analyzed in duplicate to assess heterogeneity of a sample powder aliquant. The sensitivities in each analysis using the Agilent 7500 were 6.7–9.0 × 10^4 cps/ppb for mass 89, 4.1–5.6 × 10^4 cps/ppb for mass 140 and 2.5–3.9 × 10^4 cps/ppb for mass 205. The argide production rate measured from $^{61}Ni^{40}Ar/^{61}Ni$ was 0.9–1.0 × 10^{-4}. The duplicate (second sample) was re-analyzed by an Agilent 7700x quadrupole ICP-MS, which provided higher sensitivity of 1.5–2.3 × 10^5 cps/ppb for mass 89, 140 and 205 and a lower argide production rate of 0.4 × 10^{-4} than the Agilent 7500 ICP-MS.

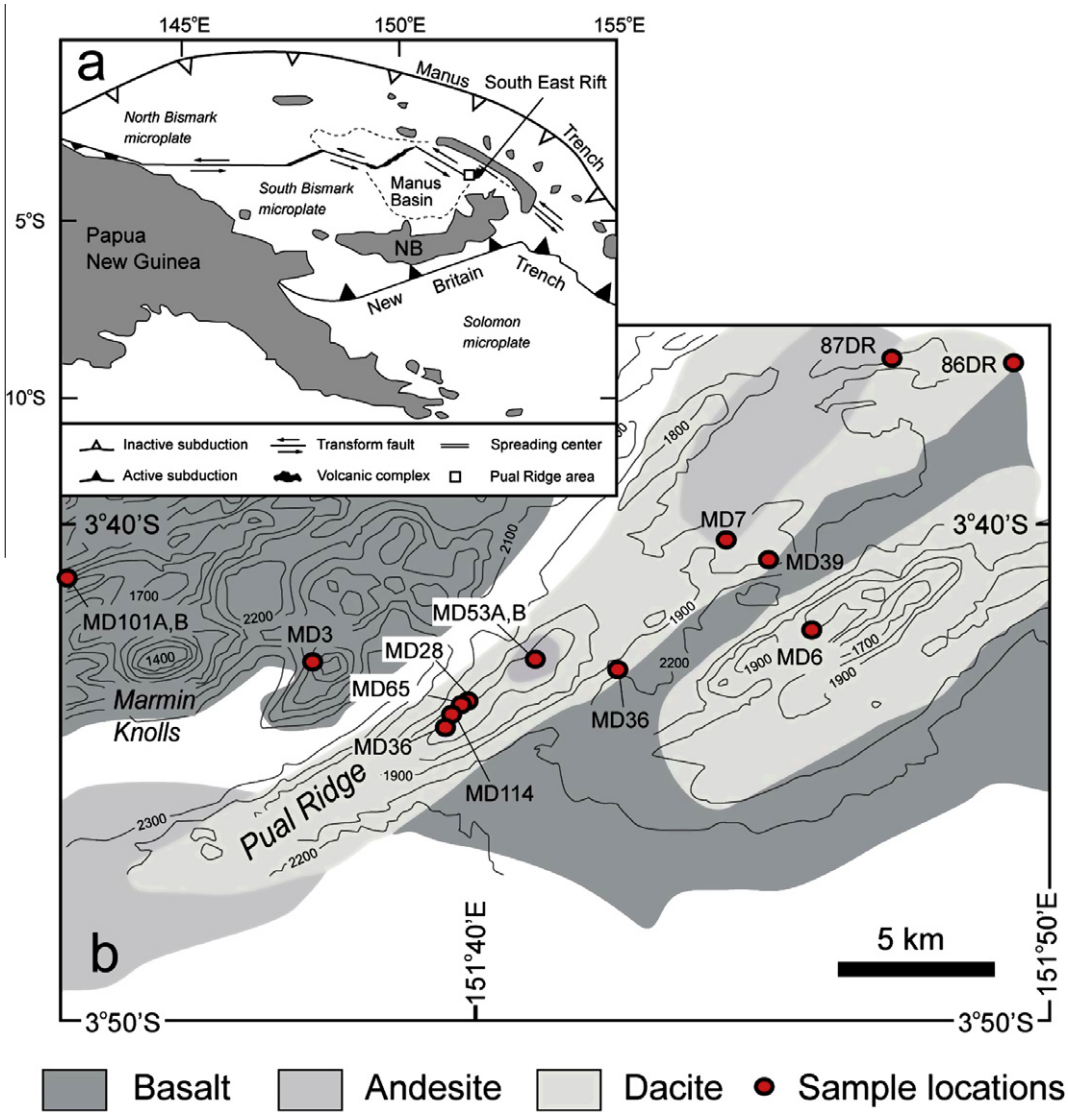

Fig. 1. (a) Simplified tectonic setting of the Manus Basin region behind the New Britain (NB) arc (modified after Taylor et al., 1994). The Pual Ridge area is shown as a small open square. (b) Bathymetric map of the Pual Ridge area, the South East Rift of the Eastern Manus Basin (modified after Moss et al., 2001 and Kamenetsky et al., 2001). Red circles represent the sample locations reported in Moss et al. (2001) and Sun et al. (2004). Contour interval is 100 m. (For interpretation of the references to color in this figure legend, the reader is referred to the web version of this article.)

Possible molecular interferences on the analyzed isotopes were monitored by measuring interference solutions of Ni, Cu, Zn, Co, Hf, Mo, Zr and Ta. The effects of the interference were subtracted using measured oxide and argide production rates. The correction is <0.5% for all PGE except for Ru. The correction rates for the Ni-argide interference on Ru were generally less than 50% except for two analyses of MD6 and MD7 where the correction factor was 80% and 140%, respectively. However, the good reproducibility for Ru in MD6 suggests that the correction is reliable (Table 1). Samples with high Ru corrections (>50%) are indicated in italic in Table 1. Concentrations of Ir, Ru, Pt, Pd and Re were determined by isotope dilution. Concentrations of monoisotopic Rh were corrected by a method described in Meisel et al. (2003) and Park et al. (2012c).

A potential disadvantage of the conventional (without isotope dilution) Ni–sulfide fire assay technique is the possibility of incomplete PGE yields relative to Carius Tube digestion (e.g. Puchtel et al., 2004). However, a direct comparison of the two methods revealed no marked systematic differences in recovery (Barnes and Fiorentini, 2008; Savard et al., 2010). Moreover, Ni–sulfide fire assay technique used here is insensitive to the absolute yield for those element concentrations that are determined by isotope dilution.

Procedural blanks were determined from sample-free analyses using 2 g of sodium borax, 0.2 g of Ni and 0.1 g of S for every session. Average procedural blanks based

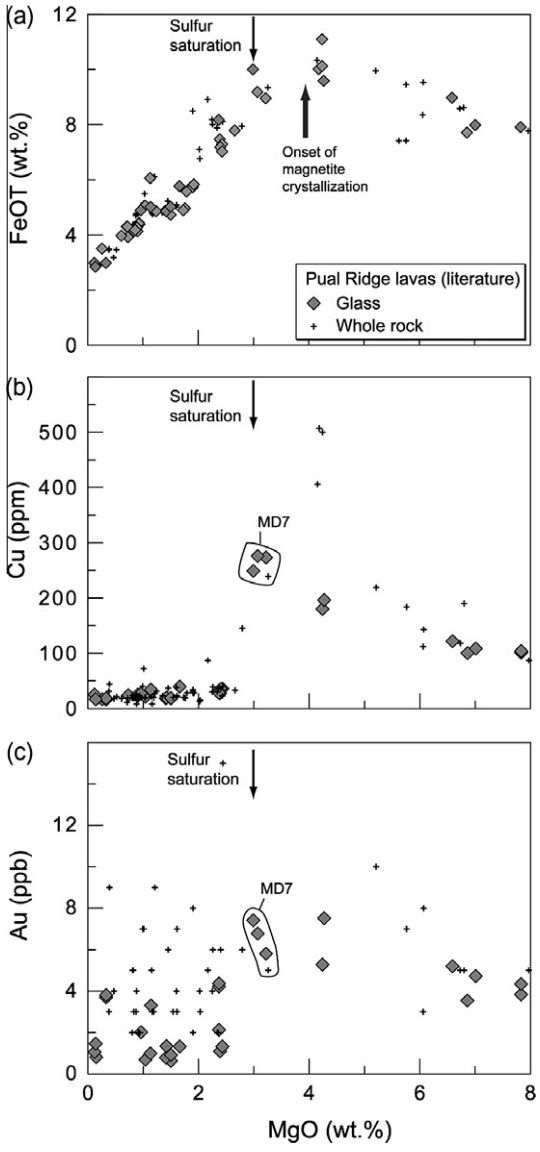

Fig. 2. Binary plots of (a) total FeO, (b) Cu and (c) Au against MgO for the Pual Ridge lavas using data taken from the literature. Sun et al. (2007) and Jenner et al. (2010) analyzed Cu and Au in glasses by *in situ* LA-ICP-MS (diamonds) whereas Moss et al. (2001) and Park et al. (2010) analyzed whole rock Cu and Au by solution ICP-MS (crosses).

on five analyses were 0.5 ± 0.3 ppt for Ir, 1.1 ± 0.9 ppt for Ru, 0.8 ± 0.4 ppt for Rh, 16 ± 17 ppt for Pt, 12 ± 5 ppt for Pd and 10 ± 5 ppt for Re (1σ). All the PGE and Re data reported in Table 1 are blank subtracted. The method detection limits (MDL), taken to be three standard deviations of the procedural blanks, were 0.8 ppt for Ir, 2.6 ppt for Ru, 1.2 ppt for Rh, 52 ppt for Pt, 15 ppt for Pd and 16 ppt for Re. The uncertainty in the PGE and Re data comes mainly from the uncertainty in the blank subtraction and ICP-MS counting statistics. Uncertainties are better than 10% unless otherwise shown in Table 1. Accuracy and precision of analyses were assessed by replicate analyses of the reference material TDB-1 (CANMET diabase) (Table 2). The TDB-1 analyses gave reproducibilities of RSD <8% for all PGE and Re except Ir (14%) and the data agree with the values reported by Meisel and Moser (2004) and Peucker-Ehrenbrink et al. (2003) within error (2σ).

4. RESULTS

The PGE and Re data for the Pual Ridge lavas are given in Table 1. The high-Mg lavas contain 7.6–21.0 ppb Pd and 0.28–1.09 ppb Re. The abundances of these elements increase with decreasing MgO between 8 and 3 wt.% (Fig. 3a and b), which mimics the trends for Cu and Au observed in the previous studies (Fig. 2b and c). The high-Mg lavas have 0.004–0.146 ppb Ir, 0.010–0.638 ppb Ru, 0.105–0.385 ppb Rh, and 1.13–7.61 ppb Pt. The abundance of these elements decreases with decreasing MgO, which is the opposite of the trends shown by Pd, Re, Cu and Au (Figs. 3c–f and 2b and c). In contrast, Pd and Re show positive correlations with MgO in the low-Mg lavas behaving similarly with Pt and Rh, although Ir and Ru do not show any correlation (Fig. 3). Our Re data are consistent with the literature values (Sun et al., 2003; Jenner et al., 2010), whereas Pt data are lower than those from Jenner et al. (2010). The differences in Pt values are discussed in Appendix A.

Primitive mantle (PM)-normalized PGE and Re patterns for the Pual Ridge lavas are shown in Fig. 4. The patterns and absolute PGE abundances of the high-Mg lavas are comparable to those of arc picritic lavas from Grenada, Lesser Antilles arc and Ambae, Vanuatu arc (Woodland et al., 2002; Park et al., 2012a), although the Pual Ridge high-Mg lavas are enriched in Pd compared to the other arc picritic lavas. The low-Mg lavas are depleted in all PGE relative to the high-Mg lavas showing MORB (mid-ocean ridge basalt)-like abundances whereas Re concentrations are similar in both the high-Mg and low-Mg lavas. The significant depletion of highly chalcophile PGE relative to weakly chalcophile Re in the low-Mg lavas suggests that the magma have reached sulfur-saturation during crystallization.

5. DISCUSSION

5.1. Pt-alloy saturation in the high-Mg lavas (>3 wt.% MgO)

Palladium and Re data exhibit negative correlations with MgO between 8 and 3 wt.%, indicating that these elements are incompatible and excluded from early crystallizing phases such as olivine, plagioclase and clinopyroxene (Fig. 3a and b). In contrast, the concentrations of Ir, Ru, Rh and Pt are positively correlated with MgO between 8 and 3 wt.% (Fig. 3c–f), showing that these elements were compatible during magma differentiation with bulk distribution coefficients >1. This hypothesis is consistent with the observation that phenocryst-bearing lavas, MD3-p and MD101A-p, are significantly enriched in Ir, Ru, Rh and Pt compared to the corresponding glassy lavas, MD3 and MD101A, whereas for Pd and Re there is no significant difference (Fig. 3 and Table 1).

The effect of fractional crystallization on the PGE and Re abundances of the high-Mg lavas was investigated by

Table 1
Concentrations of MgO, Yb, Cu, Au, Re and PGE of the Pual Ridge lavas.

Sample	MgO[a]	Yb[a]	Cu[a]	Au[a]	Re	Pd	Pt	Rh	Ru	Ir
MD3[b]	7.83	1.35	103	3.84	0.382	7.61	2.80	0.187	0.288	0.070
MD3-p[b]	7.83	1.35	103	3.84	0.284	10.4	7.61	0.385	0.638	0.146
MD101A	7.01	1.41	109	4.73	0.302	13.0	3.40	0.207	0.092	0.046
MD101A-p	7.01	1.41	109	4.73	0.394	12.7	5.71	0.265	0.125	0.094
MD101B	6.59	1.67	122	5.20	0.308	13.7	3.20	0.198	0.073	0.036
MD101B	6.59	1.67	122	5.20	0.346	12.9	3.32	0.208	0.076	0.035 ± 6
86DR	4.27	2.38	196	7.52	0.685	20.0	1.13	0.105	0.010 ± 5	0.0051 ± 8
86DR[b]	4.27	2.38	196	7.52	1.09	21.0	1.36	0.126	0.011 ± 4	0.0043
MD7	2.99	2.73	249	7.42	1.33	1.94	0.843	0.0088	<0.0026	<0.0008
MD7[b]	2.99	2.73	249	7.42	1.63	2.12	0.927	0.0059 ± 12	*0.0028 ± 18*	0.0012 ± 4
MD53A	2.37	3.44	30	3.57	0.902	1.03	0.371	0.023	0.0090 ± 21	0.046
MD53A[b]	2.37	3.44	30	3.57	1.44	1.41	0.410	0.030	0.0072 ± 13	0.023
MD53B	1.66	3.44	40	1.33	1.53 ± 26	0.160 ± 20	<0.052	0.0026 ± 7	<0.0026	<0.0008
MD53B[b]	1.66	3.44	40	1.33	1.18	0.175	0.084 ± 24	0.0026	<0.0026	<0.0008
MD36	1.50	3.96	27	2.02	1.36 ± 41	0.146 ± 16	0.095 ± 20	0.0037 ± 23	<0.0026	0.0011 ± 5
MD36[b]	1.50	3.96	27	2.02		0.042	0.075	0.0027 ± 7	<0.0026	<0.0008
MD28	1.42	3.58	34	3.31	0.661	0.561	0.360	0.020 ± 2	0.013 ± 2	0.0071 ± 9
MD28[b]	1.42	3.58	34	3.31	0.758	0.671	0.333	0.020	0.013	0.0072
MD65	1.14	3.89	20	1.35	0.787 ± 89	0.522	0.315	0.029	0.019	0.011 ± 2
MD65[b]	1.14	3.89	20	1.35	0.568	0.740	0.254	0.021	0.012	0.0060
MD114	0.96	3.39	19	0.92	0.763	0.051 ± 13	0.121 ± 19	0.016 ± 2	<0.0026	0.0084 ± 11
MD114[b]	0.96	3.39	19	0.92	0.805	0.137	0.162	0.0062	<0.0026	0.0095
MD39	0.33	4.31	25	1.06	0.486	<0.015	<0.052	0.0079 ± 12	<0.0026	<0.0008
MD39[b]	0.33	4.31	25	1.06	0.575	<0.015	<0.052	0.0038	<0.0026	<0.0008
MD6	0.14	4.37	17	3.70	0.616	0.033 ± 9	0.062 ± 19	0.0058 ± 8	*0.0053 ± 11*	0.0018 ± 11
MD6[b]	0.14	4.37	17	3.70	0.635	0.047	0.060 ± 32	0.0054 ± 15	0.0040 ± 27	0.0015 ± 4
87DR	0.12	4.73	17	1.47	0.356	0.041 ± 7	<0.052	0.0043 ± 12	<0.0026	<0.0008
87DR[b]	0.12	4.73	17	1.47	0.367	<0.015	<0.052	0.0022	<0.0026	<0.0008

Notes: MgO is in weight percent, Yb and Cu are in ppm, Au, Re and PGE are in ppb, Analytical uncertainties >10% are specified as 1σ. All the samples were analyzed in duplicate, using different powder aliquots. MD3-p and MD101A-p are phenocryst-bearing samples (~10% modal). Ruthenium data with high interference corrections (>50%) are indicated in italic.

[a] Data from Sun et al. (2007).

[b] Average of two analyses obtained using Agilent 7500 and Agilent 7700x. The analyses were performed using the same sample solution. Raw data are presented in Appendix B.

Table 2
PGE and Re analyses of TDB-1 (ppb).

	Re	Pd	Pt	Rh	Ru	Ir
TDB-1 (CANMET)						
#1	0.68	21.7	4.37	0.389	0.163	0.068
#2	0.72	21.1	4.14	0.360	0.139	0.052
#3	0.75	21.9	4.26	0.382	0.153	0.064
Average ($n = 3$)	0.72 ± 0.08	21.6 ± 0.8	4.26 ± 0.23	0.377 ± 0.030	0.152 ± 0.023	0.061 ± 0.017
M&M[a] ($n = 7$)	0.79 ± 0.04	24.3 ± 3.4	5.01 ± 0.34	0.471 ± 0.078	0.198 ± 0.016	0.075 ± 0.018
P[b] ($n = 8$)		24.8 ± 1.4	4.40 ± 0.30			0.078 ± 0.006
Certified[c]		22.4	5.80	0.70	0.30	0.150

Reproducibilities are quoted at 2σ.

[a] Meisel and Moser (2004), high pressure asher (HPA) digestion ID-ICP-MS.

[b] Peucker-Ehrenbrink et al. (2003), Ni–sulfide fire assay ID-ICP-MS.

[c] Govindaraju (1994), note that Ir, Ru and Rh values are provisional values.

calculating the bulk distribution coefficients (D) for PGE and Re between the melt and the crystallizing phases (e.g. Momme et al., 2002). Since the Pual Ridge lavas evolved dominantly by fractional crystallization (Jenner et al., 2010 and references therein), we used the fractional crystallization equation, $C/C_o = F^{(D-1)}$ to calculate the bulk D required to model the variations of PGE and Re with magma evolution, where C is the concentration of an element of the sample, C_o is the concentration of the element of the most primitive lavas (>7 wt.% MgO), F is the fraction of melt remaining, and D is bulk distribution coefficient of the fractionating assemblage. Yb was used to calculate F by setting C_o^{Yb} to the Yb

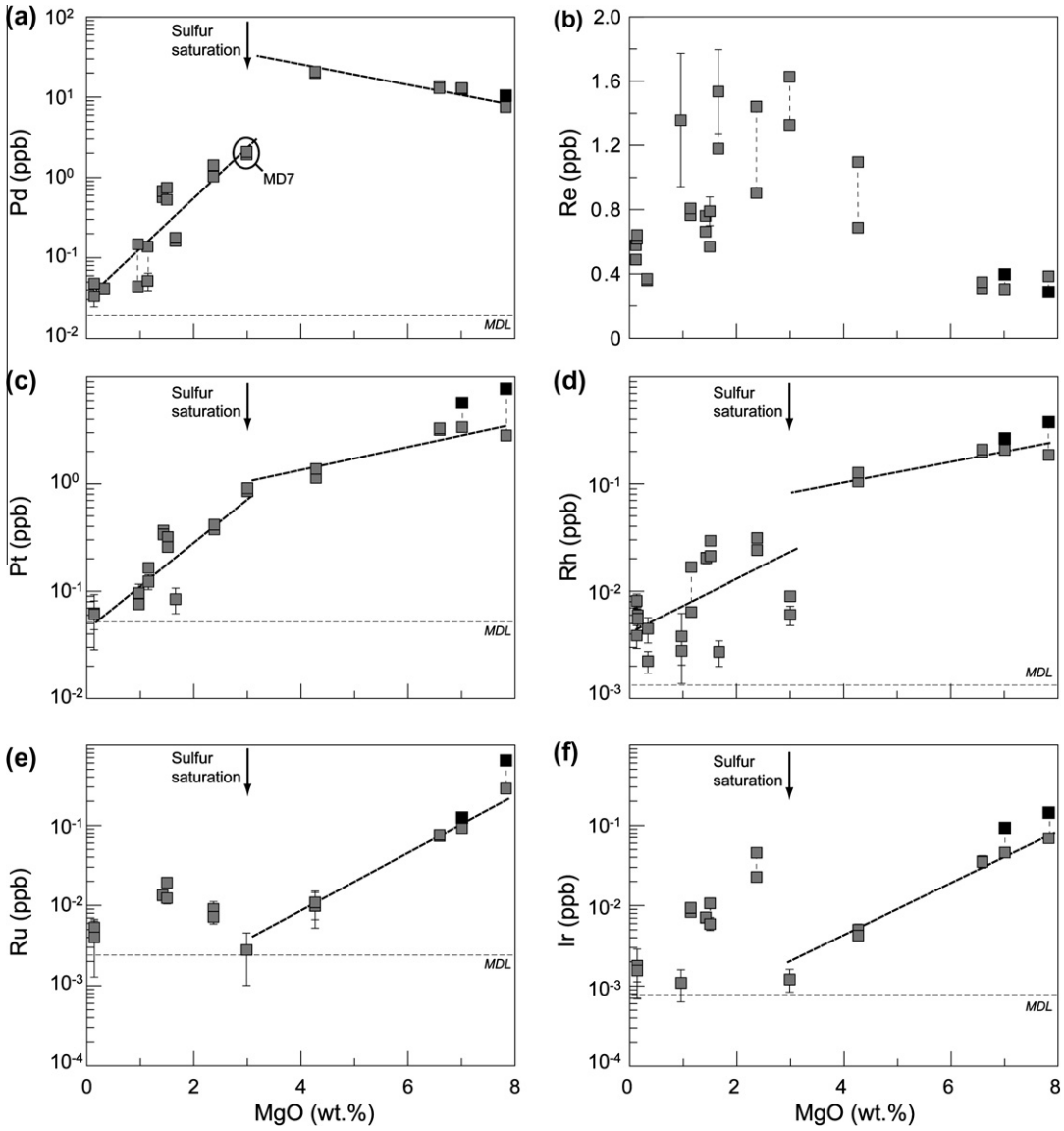

Fig. 3. (a–f) Binary plots of PGE and Re against MgO for the Pual Ridge lavas. Vertical dashed lines connect duplicate analyses. Thick dashed lines are nonlinear exponential least square fits for the high-Mg and the low-Mg glassy lavas. Black squares represent phenocryst-bearing samples. Note that phenocryst-bearing lava samples are enriched in Ir, Ru, Rh and Pt, but not Pd and Re compared to corresponding glassy lava samples. Method determination limits for each element (MDL) are presented as horizontal dashed lines.

concentration in MD3 (1.35 ppm; Sun et al., 2007), which is the most primitive Pual Ridge sample analyzed in the present study. F was calculated using $D_{Yb} = 0.33$, which assumes fractionation of clinopyroxene, plagioclase and olivine in the proportions of 60:35:5 and partition coefficient values for these minerals from Fujimaki (1986). These proportions of silicate minerals best explain major element variations of the high-Mg lavas and a change in the proportions does not significantly affect our model since each mineral does not have a strong affinity for the PGE and Re. The calculated F values based on Yb were then used to calculate bulk D values for the PGE and Re. Calculated PGE and Re variations with F for the high-Mg lavas are shown in Fig. 5. Palladium and Re are progressively enriched in the melt as magma evolves and can be modeled with a bulk *D* value of 0.2 and 0.01, respectively (Fig. 5a and b), which is similar to those of Cu and Au (D = 0.2; modeled using data from Sun et al., 2007). The incompatible behavior of Cu, Au and Pd reflects sulfide-undersaturated magma evolution of the high-Mg lavas. The compatible behavior of Ir, Ru, Rh and Pt can be modeled using D values of 3–3.8, 5, 1.2–1.7 and 1.2–2.2, respectively (Fig. 5c–f). Iridium and Ru are more efficiently removed from the melts than Rh and Pt and require the highest D values.

We modeled the fractional crystallization of clinopyroxene, plagioclase and olivine to investigate the effect of these minerals on PGE and Re variations in the high-Mg lavas using partition coefficient values reported in the literature (Table 3). Model 1 shows the effect of olivine + plagioclase + clinopyroxene fractional crystallization on PGE abundances (Fig. 5). The model can explain the variations

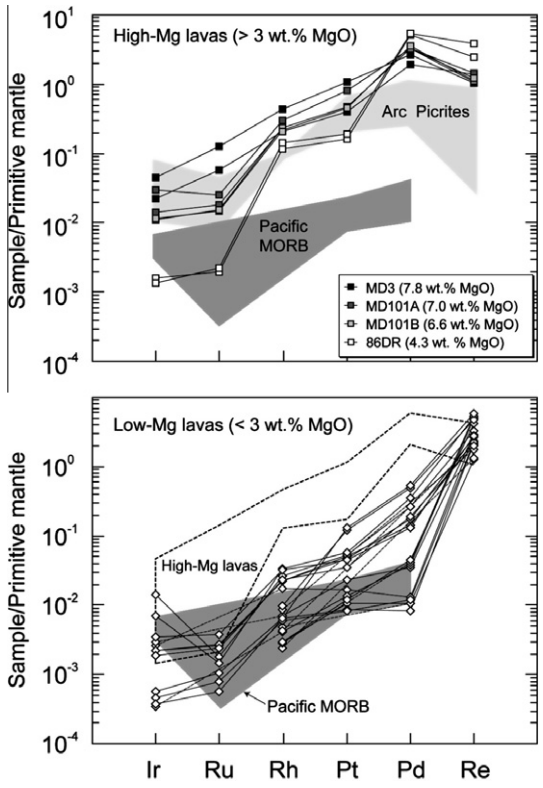

Fig. 4. Primitive mantle-normalized PGE and Re concentrations of the Pual Ridge lavas. Normalizing values from McDonough and Sun (1995). Arc picrites and Pacific MORB field are also shown for comparison. The Pacific MORB field is based on the data from Bezos et al. (2005). The arc picrites (>10 wt.% MgO) field is based on data from Woodland et al. (2002) and Park et al. (2012a).

of Pd and Re however it cannot account for the Ir, Ru, Rh and Pt variations, which requires a phase containing significant Ir, Ru, Rh and Pt.

The higher PGE concentrations of phenocryst-bearing lavas (MD3-p and MD101A-p) compared with their glassy equivalents (MD3 and MD101A) suggest the presence of a PGE-rich microphase, associated with the phenocrysts, in the high-Mg lavas (Table 1 and Fig. 3). This hypothesis is consistent with the variations of Ir, Ru, Rh and Pd against Pt in the high-Mg lavas (Fig. 6). The strong positive correlations between Ir, Rh and Pt, to some extent Ru, suggest that these elements are contained within a single mineral in similar proportions. It should be noted that Pd does not show any correlation with Pt, indicating that the phase in question does not contain a significant amount of Pd (Fig. 6d).

Cr spinel, PGE-rich alloy and laurite (RuS_2) have been considered to be dominant hosts for PGE in ultramafic–mafic magmas in sulfide-undersaturated conditions. However, Cr spinel and laurite cannot explain the compatible behavior of Pt observed from the high-Mg lavas, although it may account for IPGE (Ir-group PGE; Os, Ir, Ru) variations, because Pt is incompatible with these minerals (Brenan and Andrews, 2001; Brenan et al., 2012; Park et al., 2012a). There have been a number of suggestions that crystallization of an Ir-rich alloy controls PGE variations in mafic–ultramafic magmas (Barnes et al., 1985; Brügmann et al., 1987; Greenough and Fryer, 1990; Rehkämper et al., 1999; Philipp et al., 2001; Momme et al., 2002; Puchtel et al., 2004; Barnes and Fiorentini, 2008; Ireland et al., 2009; Pitcher et al., 2009; Song et al., 2009) and the Ir-rich alloy may contain some Pt (e.g. Peck et al., 1992; Brenan and Andrews, 2001; Song et al., 2009). However, all of these studies showed that Pt behaves primarily as incompatible elements during the evolution of an Ir-rich alloy saturated magma. As a consequence, an Ir-rich alloy is unlikely to be the phase responsible for the PGE variations in the high-Mg lavas in which Pt behaves as a compatible element. Fig. 7 compares Pd/Pt and Pt/Ir of the Pual Ridge high-Mg lavas and volcanic suites that have fractionated an Ir-rich alloy. The Pd/Pt markedly increases with a moderate increase of Pt/Ir during magma evolution in the Pual Ridge high-Mg lavas. This trend is clearly distinguishable from that of Ir-rich alloy crystallization, which are characterized by a relatively constant Pd/Pt and a marked increase in Pt/Ir. This suggests crystallization of a Pt-rich phase in the high-Mg lavas and the most likely phase to host Ir, Ru, Rh and Pt without Pd is a Pt-rich alloy. Evidence for Pt-rich alloy crystallization occurs in several ultramafic–mafic complexes and primitive arc lavas (Spandler et al., 2000, 2003; Garuti et al., 2002, 2003; Augé et al., 2005; Zaccarini et al., 2011; Park et al., 2012a), although it has not been widely reported.

The formation of the Pt-rich alloy results from the low solubility of Pt in silicate melts, which varies as a function of fO_2 and temperature (Fortenfant et al., 2003; Borisov and Palme, 1997; Ertel et al., 1999). Liquidus temperatures of the high-Mg lavas, as calculated using the equation described in Sugawara (2000) at 1 kbar and 1.0 mol% H_2O, range between 1100 °C and 1200 °C. The oxygen fugacity of the high-Mg lavas has been suggested to be $fO_2 =$ QFM + 2.0 (Jenner et al., 2010). The Pt solubility in an anorthite-diopside synthetic melt under these conditions can be calculated from the equation of Fortenfant et al. (2003) and is compared with the abundances of Pt in the high-Mg lavas in Fig. 8. The estimated Pt solubility curve is about 20% higher than the Pt contents in the high-Mg lavas (Fig. 8). However, it should be noted that all Pt solubility experiments were carried out in Fe-free synthetic melt. In natural Fe-bearing systems, Pt solubility will be significantly lower because Pt has a strong affinity for Fe, which will lower the activity of Pt required for alloy saturation (Borisov and Palme, 2000). Similarly, incorporation of other PGE in the alloy will further lower the Pt solubility. Therefore, it is highly likely that the high-Mg Pual Ridge melt was Pt–Fe alloy-saturated.

If it is assumed that the differences in PGE abundances between glassy lavas and phenocryst-bearing lavas result solely from the presence of Pt-rich alloy nuggets in the phenocryst-bearing lavas, we can estimate the composition of the Pt-rich alloy by subtracting PGE abundances in a glassy lava from the PGE abundances in a corresponding phenocrysts-bearing lava, and normalizing the result to 100 wt.%. Table 4 shows the estimated compositions of the Pt-rich alloys. The compositions calculated from MD3 and MD101A are broadly similar, except for Ru. These estimates are reasonably in agreement with the compositions of magmatic Pt-rich alloys (e.g. isoferroplatinum: Pt_3Fe) from picritic

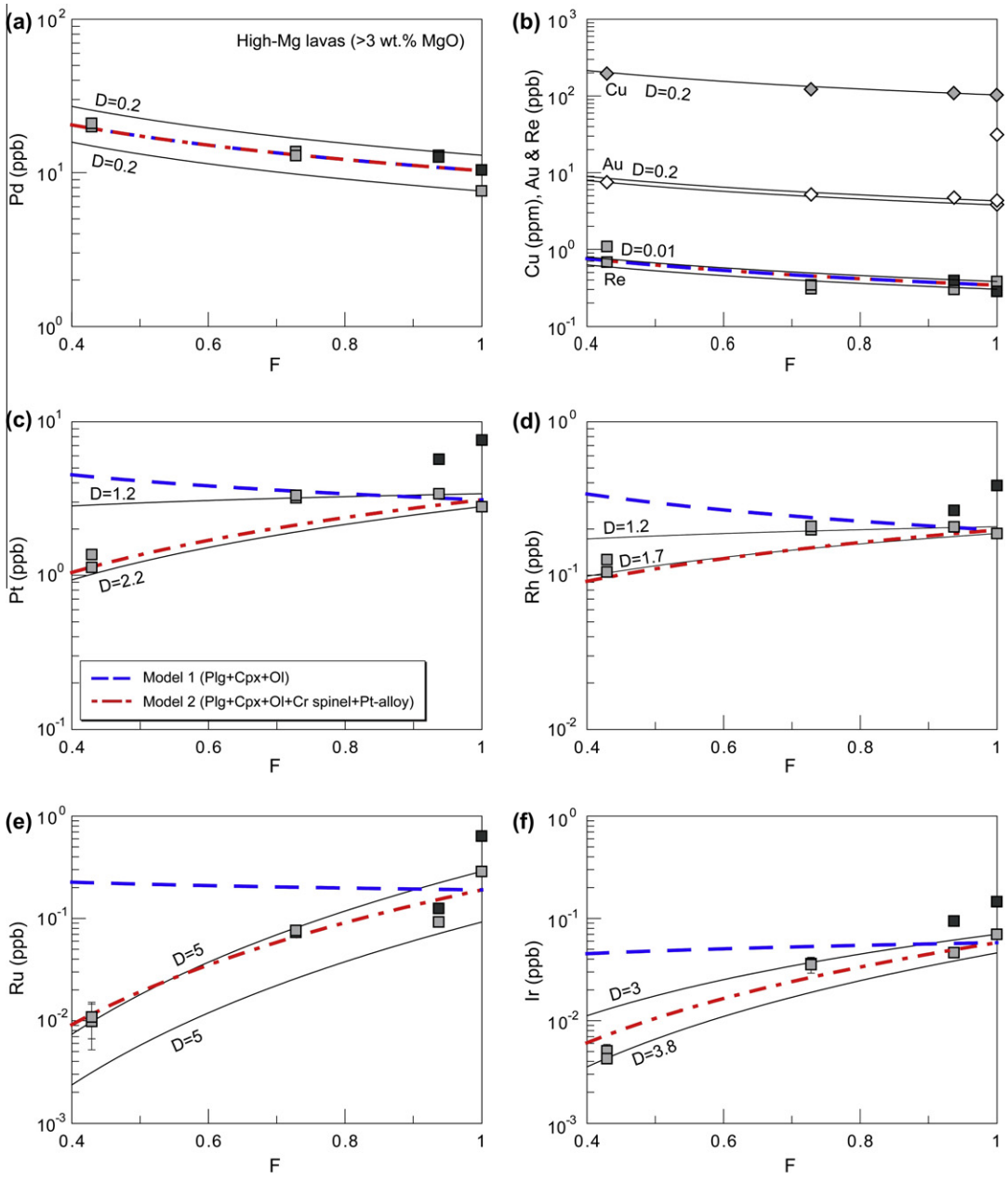

Fig. 5. (a–f) Binary plots of PGE, Re, Cu and Au concentrations of the high-Mg lavas as a function of F, the remaining melt fraction (see text for discussion). Black squares represent phenocryst-bearing samples. Solid lines are calculated fractional crystallization models based on the composition of the high-Mg lavas. Bulk partition coefficients, D, used in the models are shown on the diagram. The range of PGE, Re and Au concentrations of sample MD3 and MD101A were used as varying initial concentrations for the models. Model 1 represents fractional crystallization trends for clinopyroxene + plagioclase + olivine (60:35:5), and Model 2 represents fractional crystallization trends of silicate minerals + Pt-rich alloy + Cr spinel with an alloy fraction of 6×10^{-7}% and a Cr spinel fraction of 0.1%. The average concentrations of PGE of MD3 and MD101A were used as the initial concentrations for the models. Models 1 and 2 are identical for Pd and Re.

lavas, Vanuatu (Park et al., 2012a), chromitites of the Kytlym and Uktus complexes, Northern and Central Urals (Garuti et al., 2002), and dunites of the Greenhills complex, New Zealand (Spandler et al., 2003), which strongly suggest the presence of a Pt-rich alloy along with phenocrysts. However, Ru values in the present study, which range from 1.2 to 5.8 wt.%, are higher than the literature values of <0.5 wt.%. This represents the presence of a Ru-rich phase that occurs with the Pt-rich alloy in the accumulated phenocrysts. As a possible Ru-rich phase one may consider laurite or Cr spinel. However, given the high thermal stability of laurite >~1250 °C (Brenan and Andrews, 2001) and the low Ru concentrations in the high-Mg lavas, laurite crystallization is unlikely in the high-Mg lavas. In contrast, Cr spinel inclusions were commonly observed in olivine phenocrysts from Pual Ridge lavas (e.g. Kamenetsky

Table 3
Crystal/melt partition coefficients for the modeling of the Pual Ridge lavas.

	Pd	Pt	Rh	Ru	Ir	Re	Cu	Reference[a]
Olivine	0.005	0.009	2.59	2.19	1.7	0.009		1
Clinopyroxene	0.3	0.8	0.23	1.0	1.8	0.002	0.66	2
Cr spinel	0.032	0.22	641	2448	472	0.0012		3
Plagioclase	0.2	0.3	0.4	0.3	0.3	0.01[b]	0.37	4
Magnetite	1.1	0.22				26	1.6	5
Sulfide	4600[c]	4000[c]				0.01	1000	6

[a] References for partition coefficients data are as follows: 1 = Brenan et al. (2003, 2005), Mallmann and O'Neill (2007); 2 = Capobianco and Drake (1990), Capobianco and Drake (1994), Ewart and Griffin (1994), Hill et al. (2000), Righter et al. (2004), Chazey and Neal (2005), Mallmann and O'Neill (2007); 3 = Righter et al. (2004), Brenan et al. (2012), Park et al. (2012a); 4 = Capobianco and Drake (1994), Ewart and Griffin (1994), Chazey and Neal (2005); 5 = Capobianco et al. (1994), Ewart and Griffin (1994), Righter et al. (1998), Brenan et al. (2012); 6 = Fonseca et al. (2007), Ripley et al. (2002).
[b] Values are assumed due to no literature available and low compatibility of Re in plagioclase.
[c] Values are estimated using sulfide fraction of 0.002 and bulk D of Pd and Pt (See text for discussion).

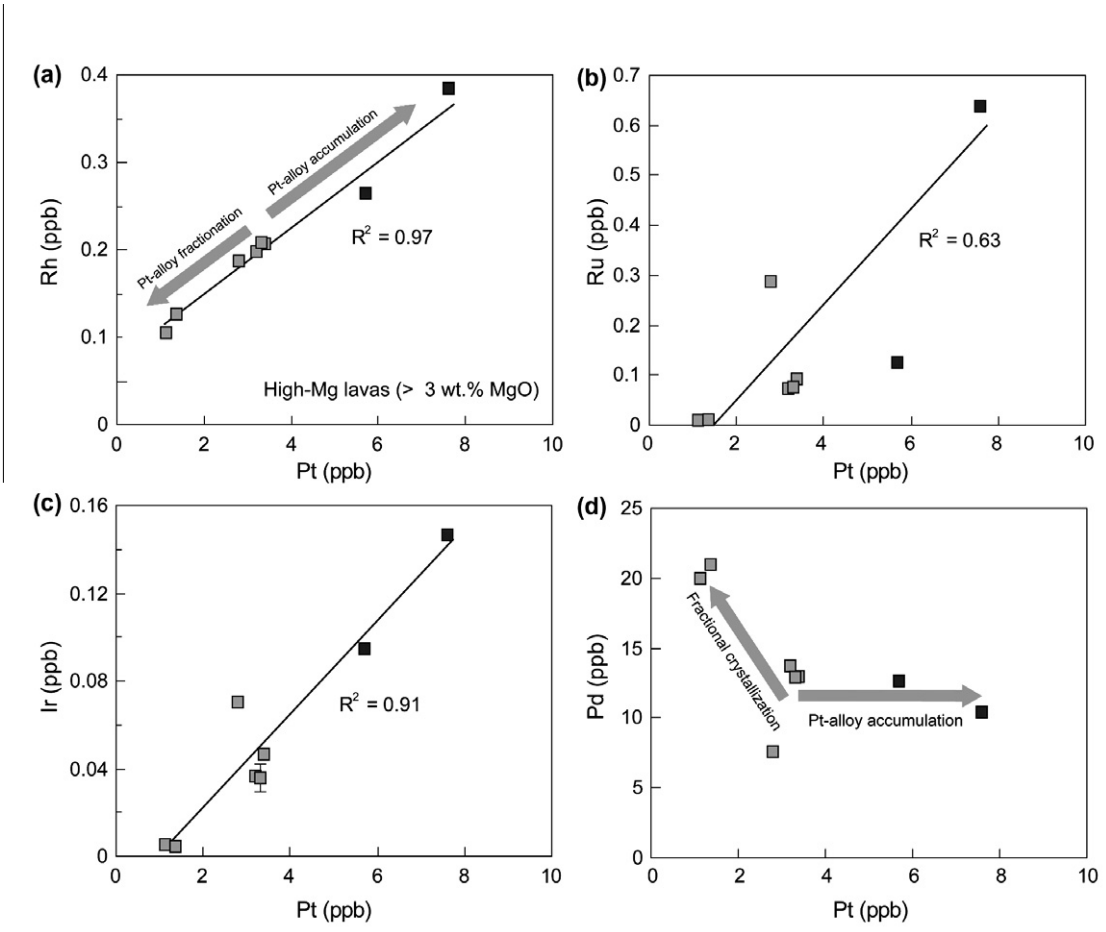

Fig. 6. Binary plots of (a) Rh, (b) Ru, (c) Ir and (d) Pd against the Pt concentrations of the high Mg lavas. Black squares represent phenocryst-bearing samples. Note that Rh, Ru and Ir show positive linear correlations with Pt whereas Pd does not show any correlation with Pt.

et al., 2001), indicating that a small fraction of Cr spinels crystallized along with olivine, although the crystallization of Cr spinel would have reduced significantly once Cr-bearing clinopyroxene (1.0–1.2 wt.% Cr_2O_3) appeared as a liquidus phase. The compatibility of Ir, Ru and Rh in Cr spinel is well documented in the literature, with the partition coefficient of Ru in Cr spinel being generally higher than those of Ir and Rh (Puchtel and Humayun, 2001;

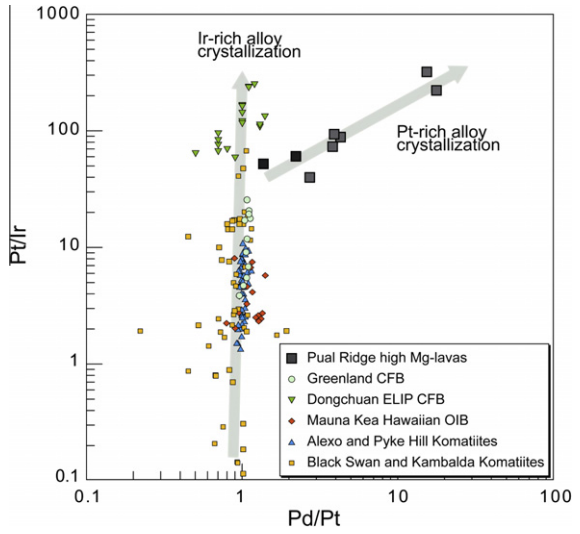

Fig. 7. A plot of Pt/Ir against Pd/Pt for the Pual Ridge high-Mg lavas and volcanic suites that have fractionated an Ir-rich alloy. PGE data compiled from: Greenland CFB = Upper section of site 917 of the Ocean Drilling Program, SE Greenland (Philipp et al., 2001), Dongchuan ELIP CFB = High Ti basalts, Emeisihan Large Igneous Province, SW China (Song et al., 2009), Mauna Kea Hawaiian OIB = Picrites and basalts from Mauna Kea, Hawaii (Ireland et al., 2009), Alexo and Pyke Hill Komatiites = Komatiites from the Alex and Pyke Hill areas, Ontario, Canada (Puchtel et al., 2004), Black Swan and Kambalda Komatiites = Komatiites from the Black Swan and Kambalda areas, South Kalgoorlie Terrane, Australia (Barnes and Fiorentini, 2008).

Puchtel et al., 2004; Righter et al., 2004; Brenan et al., 2012; Park et al., 2012a).

Partition coefficients for Ir, Ru, Rh and Pt between the Pt-rich alloy and the melt can be calculated using the PGE composition of the melt and the estimated composition of the Pt-rich alloy, and the results are presented in Table 4. In Model 2 (Fig. 5) we have added 6×10^{-7}% Pt-rich alloy and 0.1% Cr spinel as fractionating phases to Model 1 using the partition coefficients presented in Tables 3 and 4. The model fully accounts for the observed PGE variations in the high-Mg lavas.

In summary, PGE and Re variations in the high-Mg lavas can be explained by fractional crystallization of the major silicate minerals with trace amounts of Pt-rich alloy and Cr spinel. The main host phases for the compatible PGE in the high-Mg lavas are Pt-rich alloys (for Pt, Ir, Ru and Rh) and Cr spinels (for Ru, and lesser amounts of Ir and Rh).

5.2. Possible causes for chalcophile element depletion of the low-Mg lavas (<3 wt.% MgO)

The abundances of chalcophile elements such as Cu, Au and Pd decrease abruptly in the Pual Ridge lavas at 3 wt.% MgO (Sun et al., 2004; Jenner et al., 2010; this study). Sun et al. (2004) suggested that the sudden decrease of Cu and Au resulted from the escape of magmatic fluid enriched in reduced sulfur complexes. In contrast, Jenner et al. (2010) attributed the depletion to fractional crystallization of bornite. It should be noted that bornite (Cu_5FeS_4) is a crystalline Cu-rich sulfide phase, which is different from the Fe-rich sulfide immiscible melts commonly observed in a sulfide-saturated MORB magma.

In this section we will discuss how Pd and Cu behave during sulfide and fluid saturation using available data on partitioning of Pd and Cu between silicate melt, sulfide melt

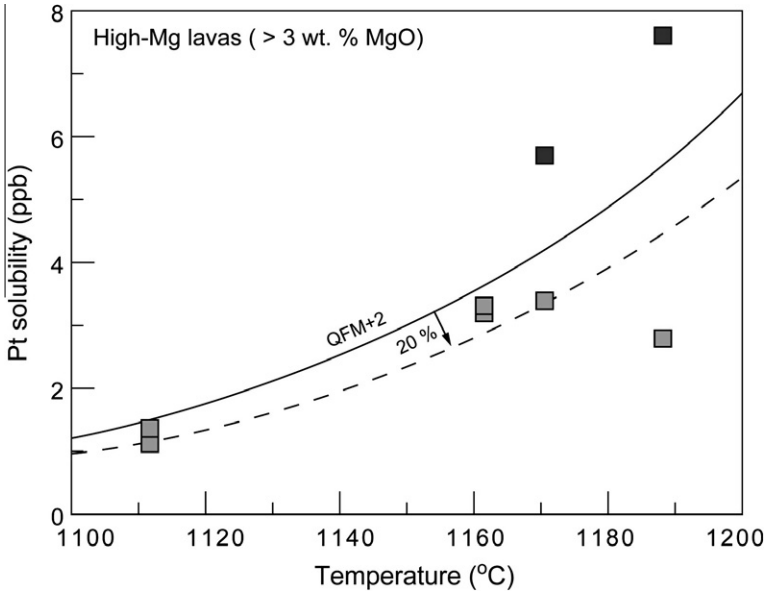

Fig. 8. Comparison between the Pt contents of the high-Mg lavas and experimentally estimated Pt solubility in Fe-free anorthite-diopside melt (Fortenfant et al., 2003). Black squares represent phenocryst-bearing samples. The solid line represents the variation of estimated maximum Pt solubility at fO_2 of QFM + 2 and 1100–1200 °C. The dotted line is 20% reduced Pt solubility curve under the same conditions. Liquidus temperatures of the high-Mg lavas were calculated using MgO contents by the equation described in Sugawara (2000) at 1 kbar and 1.0 mol% H_2O.

Table 4
Estimates of Pt-rich alloy compositions and partition coefficients.

Sample	Pt	Rh	Ru	Ir	Os	Pd	Fe	Total
MD101A	3.40	0.207	0.092	0.046	n.a.	13.0		
MD101A-p	5.71	0.265	0.125	0.094	n.a.	12.7		
Contribution from Pt-rich alloys[a]	2.31	0.058	0.033	0.048				
Estimated Pt-rich alloy composition (wt.%) [b]	84.9	2.1	1.2	1.8			10.0	100
Partition coefficient[c]	2.50×10^8	1.03×10^8	1.32×10^8	3.83×10^8				
MD3	2.80	0.187	0.288	0.070	n.a.	7.6		
MD3-p	7.61	0.385	0.638	0.146	n.a.	10.4		
Contribution from Pt-rich alloys[a]	4.81	0.198	0.350	0.076				
Estimated Pt-rich alloy composition (wt.%) [b]	79.7	3.3	5.8	1.3			10.0	100
Partition coefficient[c]	2.85×10^8	1.75×10^8	2.01×10^8	1.80×10^8				
Average partition coefficient	2.67×10^8	1.39×10^8	1.67×10^8	2.82×10^8				
Composition of Pt-rich alloys from the literature[d]								
Garuti et al. (2002) ($n = 5$)	87.0 ± 2.9	0.5 ± 0.3	0.04 ± 0.04	1.0 ± 0.8	0.5 ± 1.4	0.3 ± 0.3	8.6 ± 0.4	98.0 ± 2.4
Spandler et al. (2003) ($n = 11$)	87.8 ± 2.3	1.7 ± 0.2		1.2 ± 0.6	0.3 ± 0.2	0.4 ± 0.2	8.6 ± 0.3	100.1 ± 2.1
Park et al. (2012) ($n = 2$)	81.1–89.0	0.81–0.90	<0.1	3.0–5.4	1.6–7.7	<0.1	4.9–5.3	99.7–100.0

n.a. = Not analyzed.
[a] Calculated assuming differences between duplicate analyses are caused by Pt-rich alloy inclusions.
[b] Calculated by normalizing contribution from Pt-rich alloys to 100 wt.% assuming a Pt-rich alloy contains 10 wt.% of Fe.
[c] Calculated using the Pt-rich alloy composition estimates and PGE contents in MD101A and MD3, respectively.
[d] Errors are quoted at 1σ.

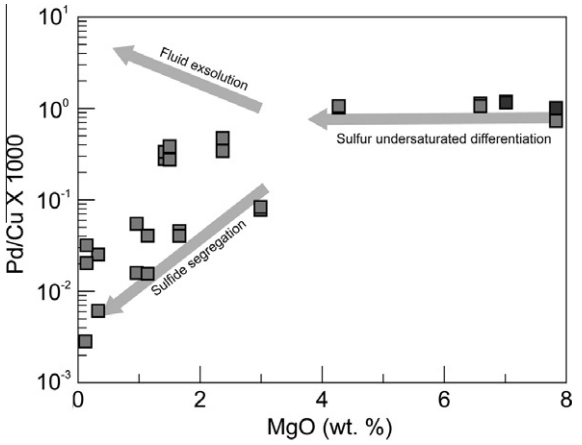

Fig. 9. A plot of Pd/Cu ratio against MgO for the Pual Ridge lavas. Note that Pd/Cu ratio falls at MgO < 3 wt.%, indicating that the decline of the ratio is due to sulfide saturation. Black squares represent phenocryst-bearing samples.

and magmatic fluid to investigate the cause of the chalcophile element depletion at 3 wt.% MgO.

Palladium and Cu behavior in sulfide-saturated magma is relatively well understood and Pd/Cu ratios have been regarded as a useful tool to identify the timing of sulfide saturation in evolving magmas (e.g. Campbell and Barnes, 1984; Barnes et al., 1988; Vogel and Keays, 1997; Philipp et al., 2001; Park et al., 2012b). This is because Pd partitions preferentially into sulfide melt relative to Cu ($D_{Pd}^{\text{sulfide-silicate melt}} > 10^5$ and $D_{Cu}^{\text{sulfide-silicate melt}} = 10^3$; Francis, 1990; Peach et al., 1990; Bezmen et al., 1994; Crocket et al., 1997; Fleet et al., 1999; Pruseth and Palme, 2004; Fonseca et al., 2009). Therefore, if a silicate melt becomes sulfide-saturated, the Pd/Cu ratio will decrease.

There are only a limited number of studies on PGE solubility in aqueous fluids at magmatic temperature (Fleet and Wu, 1993, 1995; Ballhaus et al., 1994; Hanley et al., 2005; Hanley and Heinrich, 2007). The available data suggest that PGE can be highly soluble in hypersaline aqueous fluids (20–70 wt.% eq. NaCl) at high temperature (600–1000 °C). However, Simon and Pettke (2009) reviewed the literature mentioned above and concluded that the data cannot be applied to magmatic-hydrothermal environments because the brines used in the experiments had abnormally high HCl and NaCl concentrations and there was clear evidence of disequilibrium in some of the experimental products. Simon and Pettke (2009) investigated the solubility of Pt in low-density vapor (~9 wt.% NaCl), high-density brine (~63 wt.% NaCl) and rhyolitic melts, at 800 °C and 140 MPa, which they considered to be typical of the conditions under which porphyry magmatic-hydrothermal fluids form. The partition coefficients they obtained were $D_{Pt}^{\text{vapor-melt}} = 2.9$ and $D_{Pt}^{\text{brine-melt}} = 67$. These values are 4 and 20 times lower than those for Cu at the same conditions ($D_{Cu}^{\text{vapor-melt}} = 63$, $D_{Cu}^{\text{brine-melt}} = 240$; Simon et al., 2006). Sun et al. (2007) showed that the evolution trend of Cl in the Pual Ridge lavas is best explained by low-pressure processes at about 100 MPa. At this pressure the partition coefficients of Pt become even lower ($D_{Pt}^{\text{vapor-melt}} = 1$, $D_{Pt}^{\text{brine-melt}} = 6.8$; Simon and Pettke, 2009) whereas those of Cu increase ($D_{Cu}^{\text{brine-melt}} = 700$; Williams et al., 1995). The thermodynamic study on PGE solubility in silicate melts (Wood, 1987) also suggested that the

solubility of Cu in fluid is many orders of magnitude higher than those for PGE under the same conditions. There is no detailed constraint on the solubility of Pd in such conditions. However, Pd is considered to have a similar or lower solubility than Pt in magmatic fluids (e.g. Fleet and Wu, 1993; Rehkämper et al., 1997; McInnes et al., 1999; Dale et al., 2009). Therefore, if a silicate melt becomes saturated with magmatic fluid, the Pd/Cu ratio of the residual silicate melt is likely to increase.

In the Pual Ridge lavas, the Pd/Cu remains constant during magma evolution between 8 and ~3 wt.% MgO, but it gradually decreases as the MgO content drops from 3 to 0.2 wt.% (Fig. 9). This trend implies that the high-Mg basaltic melt did not interact with sulfide melt until the MgO content of the magma fell to 3 wt.%. A continuous decrease of Pd/Cu ratio in the low-Mg lavas suggests progressive segregation of sulfide melts during the later stage of magma evolution. The Pd/Cu trend is consistent with a model whereby the depletion of Cu and Au in the Pual Ridge lavas was caused by sulfide saturation.

5.3. Effects of sulfide saturation on PGE concentrations of the low-Mg lavas (<3 wt.% MgO)

Palladium becomes compatible in the low-Mg lavas, and the abundance decreases with decreasing MgO from ~3 to 0.2 wt.% (Fig. 3a). Platinum and Rh show positive correlations with MgO as seen in the high-Mg lavas, but the slopes become steeper in the low-Mg lavas (Fig. 3c and d), which indicate changes in compatibility of Pt and Rh. Iridium and Ru do not follow the earlier trends and exhibit scattered variations against MgO (Fig. 3e and f).

In order to quantify the role of each crystallizing mineral on PGE and Re variations in the low-Mg lavas, we estimated bulk D values for Pd, Pt and Re between the melt and the crystallizing assemblage following the same procedure as for the high-Mg lavas (Fig. 10). Iridium, Ru and Rh were not examined since they do not show clear trends, which we will discuss below. We set C_o to the Yb, Pd, Pt and Re concentrations of MD7 (2.73 ppm Yb; 2.1 ppb Pd; 0.94 ppb Pt; 1.5 ppb Re), use D_{Yb} of 0.29 (Fujimaki, 1986; Gill, 1981 and references therein), and assume fractionation of plagioclase, clinopyroxene and magnetite in the proportion of 50:40:10. Model 1 (Fig. 10) shows the effect of fractional crystallization of the major silicate and oxide minerals on PGE concentrations using the partition coefficients given in Table 3. The crystallization of these minerals can account for the Re variation (Fig. 10d), however it cannot explain the variations of Pt, Pd and Cu without sulfide segregation.

After onset of sulfide saturation at 3 wt.% MgO, sulfide segregation will dominate the behavior of Pt, Pd and Cu in the low-Mg lavas. Jenner et al. (2010) suggested that the fractionating sulfide phase is a bornite crystal, which

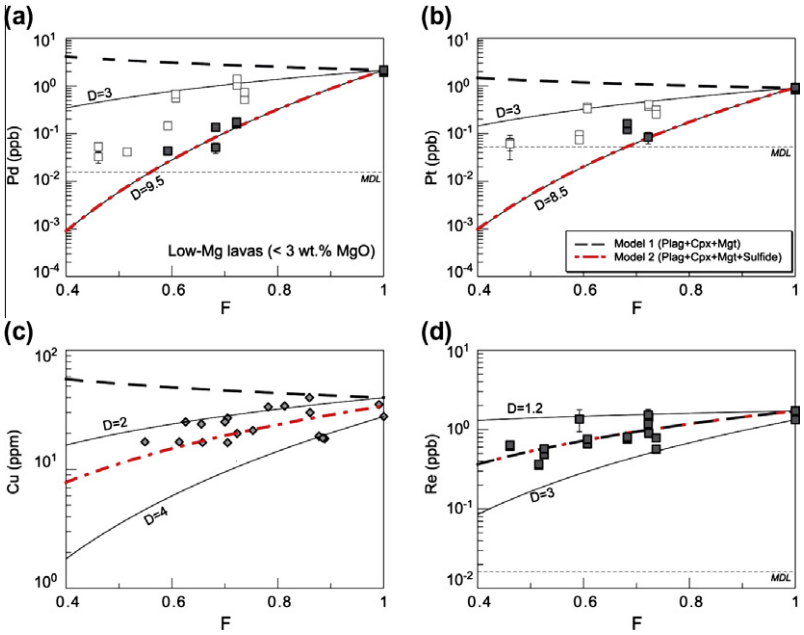

Fig. 10. Binary plots of (a) Pd, (b) Pt, (c) Cu, and (d) Re concentrations of the low-Mg lavas against F, the remaining melt fraction (see text for discussion). Cu data are from Sun et al. (2007) and Jenner et al. (2010). Open squares indicate samples that are assumed to have been contaminated by sulfide nuggets. Solid lines are calculated fractional crystallization models based on the composition of the low-Mg lavas. The ranges of Pt, Pd and Re concentrations in MD7 were used as initial concentrations for the models. Cu concentrations in the least fractionated samples after sulfide saturation were taken from literatures (Sun et al., 2007; Jenner et al., 2010) and used as initial concentrations for the models. Bulk partition coefficients, D, approximated by the model are also given on the diagram. Model 1 represents fractional crystallization trends for plagioclase + clinopyroxene + magnetite (50:40:10) and Model 2 represents fractional crystallization trends for plagioclase + clinopyroxene + magnetite + sulfide with sulfide fraction of 0.2%. Method determination limits (MDL) are shown by horizontal dashed lines.

preferentially consumed univalent Cu and Au in preference to divalent Pt and Ni. They attributed the moderate decrease of Pt and Ni to the fractionation of magnetite and silicate minerals. However, our fractional crystallization modeling, which is based on accurate and precise PGE data, shows that the Pt and Pd variations cannot be explained by fractionation of silicate and oxide minerals alone (Model 1 in Fig. 10). Instead, segregation of sulfide melts is required to explain the depletion of Pt and Pd relative to Cu and Au. Furthermore, positive inter-correlations among the PGE in the low-Mg lavas indicate that the phase sequestering Pt also contains significant amounts of Pd, Ir, Ru and Rh (Fig. 11). Therefore, the precipitating sulfide phase is likely to be immiscible sulfide liquid rather than a crystalline bornite, which is unlikely to take all PGE into its structure in the proportions required by the modeling shown above.

Therefore, if it is assumed that the sulfide melt is the host for the Pd, Pt and Cu that are unaccounted for by silicate and oxide minerals, the fraction of sulfide required to explain the variation in Cu with F is 0.2%, using $D_{Cu}^{\text{sulfide-melt}} = 1000$ (Francis, 1990; Ripley et al., 2002). This value is consistent with the estimated sulfide fraction of 0.3% in the other sulfide-saturated magma (e.g. Jamais et al., 2008). However, this fraction of sulfide requires $D_{Pd,Pt}^{\text{sulfide-melt}}$ of only $4.0–4.6 \times 10^3$ to explain the variation in Pt and Pd with F, which are at least one magnitude lower than the values of $10^4–10^8$ reported by Peach et al. (1990), Bezmen et al. (1994), Fleet et al. (1999), Crocket et al. (1997), Pruseth and Palme (2004), and Fonseca et al. (2009). We suggest that the relatively low estimates are the result of disequilibrium between the silicate and sulfide melts. Keays and Campbell (1981) suggested that when the rate of immiscible sulfide liquid separation is rapid, the ratio of the mass of the silicate melt in effective equilibrium with the sulfide liquid (R-factor; Campbell and Naldrett, 1979) becomes small. If the silicate to sulfide liquid mass ratio or R-factor is smaller than D_{PGE}, the PGE partition coefficients are controlled by R and are independent of D_{PGE} (Campbell and Naldrett, 1979). That is, the calculated partition coefficients are apparent partition coefficients controlled by R, which in this case is about $\sim 4.0–4.6 \times 10^3$. The low-Mg lavas have SiO_2 contents between 57 and 78 wt.% and temperatures that are generally below 1000 °C. The combination of the high viscosity of these silica-rich, low-temperature lavas and rapid cooling may have prevented the sulfide droplets from communicating with a large volume of surrounding silicate magma.

In the low-Mg lavas, duplicate analyses of MD36, 87DR and MD114 show significant variations in PGE contents, and most low-Mg lavas contain anomalously high Ir and Ru concentrations that are even higher than the values of MD7, the least fractionated sample among the low-Mg lavas (Table 1 and Fig. 3). The positive correlations between Rh, Pt, Pd, and to some extent Ir and Ru, indicate that these elements are contained in a sulfide phase in similar proportions (Fig. 11). We suggest that the scatter in the PGE concentrations, especially for Ir and Ru, are caused by the presence of sulfide nuggets. The sulfide nugget effect is also observed in Cu and Au data from previous studies but to a lesser extent than the PGE because of their lower affinity for immiscible sulfide melts (Fig. 2b and c). In Fig. 2, Cu and Au contents from whole rock analyses (Moss et al., 2001; Park et al., 2010) are higher than the values obtained from the glassy part of the same sample (Sun et al., 2007; Jenner et al., 2010), indicating that the whole rock samples contain Au-rich sulfide blebs. Palladium and Pt are less affected by the nugget effect than Ir and Ru (Fig. 3) because of the relatively high abundances of Pd

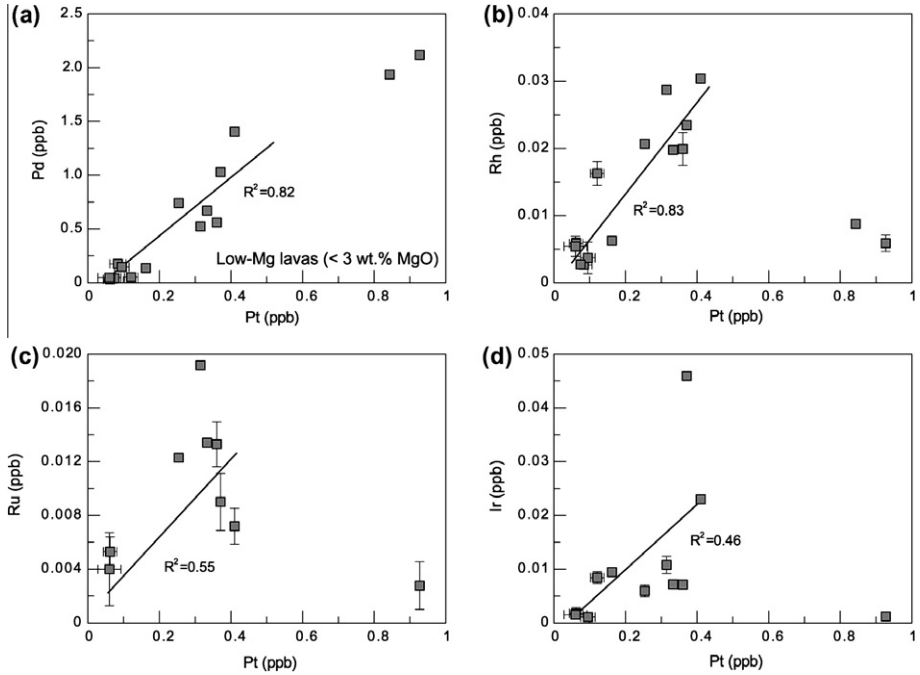

Fig. 11. Binary plots of (a) Pd, (b) Rh, (c) Ru and (d) Ir against the Pt concentrations in the low-Mg lavas. Note that All PGE show positive linear correlations with Pt. PGE concentrations of MD7 were excluded from the linear regression.

and Pt in the melts. It should be noted that the sample with the highest Cu and Au contents (MD7 in Fig. 2; Sun et al., 2007; Jenner et al., 2010) does not have the highest Pd content (Fig. 3a). This difference can be attributed to the higher compatibility of Pd compared to Cu and Au in immiscible sulfide melts (Francis, 1990; Bezmen et al., 1994; Crocket et al., 1997; Fleet et al., 1999; Pruseth and Palme, 2004; Fonseca et al., 2009). We suggest the stronger affinity for Pd in sulfide melts resulted in Pd becoming more rapidly depleted than Cu and Au in the Pual Ridge magmas from the onset of sulfide saturation.

5.4. The possible cause for Pt-rich alloy saturation in the high-Mg lavas

The PGE geochemistry of the high-Mg lavas is mainly controlled by the fractionation of a Pt-rich alloy, which is not commonly observed from the other sulfide-undersaturated magmatic systems, such as komatiites and oceanic island basalts (OIB) where PGE-bearing phases are dominantly Ir-rich alloys and/or laurites (Rehkämper et al., 1999; Barnes and Fiorentini, 2008; Ireland et al., 2009; Pitcher et al., 2009). This can be attributed to enrichment of Pt over Ir (i.e. high Pt/Ir) of the Pual Ridge lavas. The high-Mg glassy lavas contain 0.004–0.07 ppb Ir and 1.1–3.4 ppb Pt with Pt/Ir ranging between 40 and 316 whereas evolved Hawaiian OIB with similar MgO contents (7–8.5 wt.%) contain relatively high Ir (~0.19 ppb) and low Pt (~2.5 ppb) contents with low Pt/Ir (~14) (Fig. 12). Komatiites are also characterized with high Ir concentrations and low Pt/Ir (Fig. 12; Puchtel et al., 2004; Barnes and Fiorentini, 2008). This suggests that the low concentrations of Ir in the Pual Ridge lavas may have not been high enough to saturate the magma with an Ir-rich alloy whereas relatively high Pt contents and high Pt/Ir ratio result in them becoming saturated in a Pt-rich alloy at the fO_2 of ~QFM + 2 and 1100–1200 °C (Fig. 8).

There are two possible explanations for the highly fractionated chondrite-normalized PGE patterns of the Pual Ridge lavas. Firstly, the high fO_2 conditions (~QFM + 2) of the Pual ridge lavas result in the greater role of Cr spinel on PGE geochemistry than OIB and komatiites. The IPGE and Rh are compatible to Cr spinel whereas Pt and Pd are strongly incompatible, and partition coefficients for these elements between melt and Cr spinel increase with increasing fO_2, (Brenan et al., 2012; Park et al., 2012a). Therefore, the fractionation of IPGE and Rh from Pd and Pt in melts by residual Cr spinels during partial melting and fractional crystallization of Cr spinels during magma evolution must have been more efficient in the oxidized Pual Ridge magma.

Secondly, the Pual Ridge lavas may have inherited their PGE characteristics from their source. It has been suggested that Pd and Pt are selectively enriched in the sub-arc mantle by Pd and Pt-rich slab-derived fluid or melts (McInnes et al., 1999; Kepezhinskas et al., 2002; Dale et al., 2009, 2012). McInnes et al. (1999) measured PGE contents in metasomatized mantle peridotite xenoliths from Tabar–Lihir–Tanga–Lihir arc, Papua New Guinea and found that these rocks are enriched in Pt and Pd relative to surrounding depleted mantle. They suggested that Pt and Pd are more soluble in slab-derived hydrous fluids than Ir, Ru and Rh under mantle conditions and therefore these elements are selectively enriched in sub-arc mantle during metasomatism. This hypothesis is supported by a study of PGE contents in gabbros and basaltic-gabbroic eclogites from the high-pressure Zermatt-Saas ophiolite terrain, Switzerland (Dale et al., 2009). Dale et al. (2009) reported that basaltic and gabbroic eclogites are severely depleted in Pd and/or Pt compared to gabbros while Ir, Ru and Rh contents are similar each other, suggesting that Pd and Pt are selectively taken out from oceanic crust and fluxed into the sub-arc mantle from the subducting slab during transformation to eclogite. Recently, Dale et al. (2012) investigated PGE geochemistry of Tonga arc lavas and showed highly fractionated PGE patterns (Pt/Ir = 24–270) as observed in the Pual Ridge lavas. They suggest that the enrichment of Pt over Ir in the Tonga arc lavas is caused by relatively low temperature, but high degree, partial melting of depleted sub-arc mantle metasomatized by oxidized slab influx. Elevated oxygen fugacity leads to exhaustion of sulfide in the source during melting, which can explain the high Pd and Pt contents, whereas the presence of IPGE-rich alloys or laurite associated with Cr spinel can account for the low IPGE in the Tonga arc magmas (Dale et al., 2012).

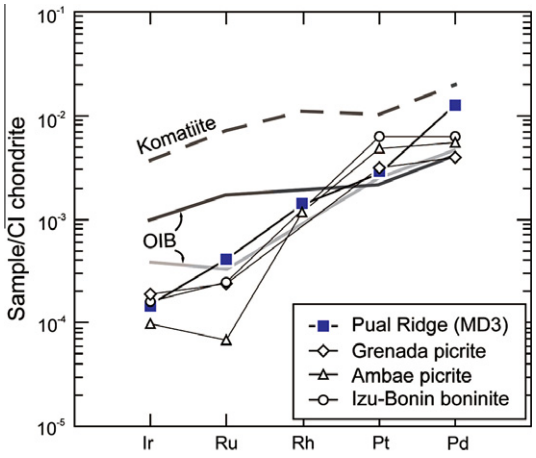

Fig. 12. Chondrite-normalized PGE concentrations of primitive magmas from different tectonic settings, including MD3, the most primitive sample analyzed in this study. Averages of PGE abundances in Grenada picrites ($n = 8$, 13–15 wt.% MgO), Ambae picrites ($n = 1$, 11 wt.% MgO) and Izu-Bonin boninites ($n = 2$, 13 wt.% MgO) are from Woodland et al. (2002) and Park et al. (2012a). The PGE abundances for parental melts of komatiites (dashed line) and Hawaiian OIB (black solid line) are also provided for comparison. The PGE composition of parental melts of komatiites and OIB were estimated by averaging the PGE data of the komatiites with 25–30 wt.% MgO ($n = 28$; Puchtel and Humayun, 2001; Puchtel et al., 2004; Barnes and Fiorentini, 2008) and by averaging the PGE abundances in OIB parental melts of Hualalai and Kilauea volcanoes (Ireland et al., 2009 and references therein), respectively. The average PGE abundances of Hawaiian basalt samples with 7–8.5 wt.% MgO (gray solid line) ($n = 8$; Ireland et al., 2009 and Pitcher et al., 2009) are also given for comparison.

The Pt-enriched and Ir-depleted feature is commonly observed in arc-related lavas (Fig. 12), despite their different partial melting conditions and mantle sources with differing slab components, suggesting the potential of Pt-alloy saturation in arc-related magmas. This is consistent with the observation that chromitites (and dunites) from arc-related cumulate complexes contain abundant Pt-rich alloys that result in positive Pt anomalies when PGE abundances for these rocks are plotted on a mantle-normalized diagram (Spandler et al., 2000, 2003; Garuti et al., 2002, 2003; Augé et al., 2005; Zaccarini et al., 2011) whereas chromitites from other tectonic settings are marked by IPGE-enriched pattern (e.g. Barnes et al., 1985).

5.5. Fractionation of Pt from Pd in evolving magmas

The PGE are sub-grouped as the Pd-group (PPGE: Rh, Pt, Pd) and the Ir-group (IPGE: Os, Ir, Ru) based on their association during magmatic processes (e.g. Barnes et al., 1985). Most mantle-derived basalts show fractionated primitive mantle-normalized PGE patterns with low Os and Ir and increasing abundances of Ru and Rh through to Pt and Pd, which indicates that the PPGE are more incompatible during partial melting and magma differentiation than the IPGE. Platinum and Pd have been thought to behave in a broadly similar manner during partial melting and fractional crystallization. However, recent studies on platinum-group minerals in mantle (Lorand et al., 1999, 2008, 2010) suggest that refractory Pt-rich alloys in the mantle may cause decoupling of Pt from Pd. Variations in Pt/Pd ratios of mantle-derived magmas have been attributed to the presence or absence of residual Pt-rich alloys in the mantle during partial melting (Brügmann et al., 1993; Maier and Barnes, 2004; Mungall et al., 2011) but the variations of Pt/Pd during magma differentiation have not been considered due to lack of evidence of a fractionating alloy phase. Our results provide the strongest evidence yet that Pt-rich alloys can crystallize from basaltic-andesitic arc-related magmas, along with silicate minerals, and fractionate Pt from Pd. The most primitive sample in this study (MD3; 7.8 wt.% MgO) is saturated with a Pt-rich alloy, which suggests that the Pual Ridge parental magma may have been Pt-rich alloy saturated at the mantle source region.

5.6. Identifying Pt-rich alloy saturation during magma differentiation

During the fractionation interval over which the Pual Ridge lavas are saturated in a Pt-rich alloy, Pd behaves as an incompatible element and its content increases in a magma while Pt is sequestered by the fractionating alloy phase and decreases in concentration (Fig. 3a and c). This observation suggests a simple method for identifying fractionation of a Pt-rich alloy. Fig. 13 shows a plot of Pd/Pt against MgO for the Pual Ridge lavas. Note that Pd/Pt increases as expected until sulfide saturation is reached then declines, showing that Pd has a higher partition coefficient into an immiscible sulfide melt than Pt. A similar trend can be identified in the Ertan high-Ti basalts from the central Emeisihan Large Igneous Province, Southwest China. In this case, the rate of increase

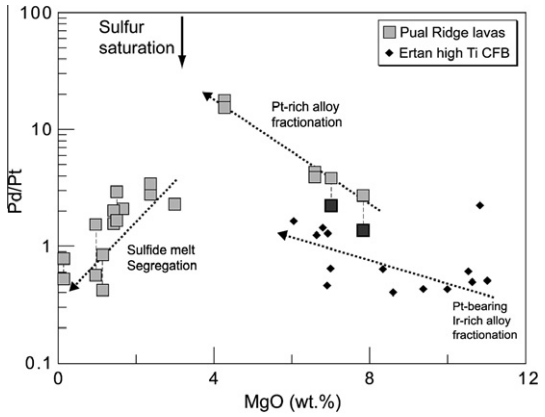

Fig. 13. A plot of Pd/Pt against MgO for the Pual Ridge lavas and the Ertan high-Ti CFB from Song et al. (2009). Vertical dashed lines connect duplicate analyses. Black squares represent phenocryst-bearing samples from the Pual Ridge lavas.

in Pd/Pt with decreasing MgO is less, because the fractionating alloy is a Pt-bearing Ir-rich alloy (Song et al., 2009). However, this approach cannot be used to identify fractionation of a Pt-poor Ir alloy. For example, Pd/Pt remains nearly constant (~1; Fig. 7) during magma evolution of mantle plume related komatiites, Hawaiian OIBs, and the Greenland and Dongchuan CFBs probably because the Ir-rich alloy does not contain enough Pt to fractionate Pt from Pd. Here, Pd/Ir may be more useful to identify alloy fractionation but we caution that an allowance must be made for Ir sequestration by olivine and Cr-rich spinel.

6. CONCLUSIONS

We have investigated the PGE and Re geochemistry of Pual Ridge lavas and found that the PGE behave differently before and after the onset of sulfide saturation. Prior to sulfide saturation Ir, Ru, Rh and Pt behave as compatible elements whereas Cu, Re, Au and Pd behave incompatibly. The phase responsible for the depletion of Ir, Ru, Rh and Pt during the early stages of fractional crystallization is an Ir–Ru–Rh bearing Pt-rich alloy. Cr spinel crystallization also contributes to the depletion of Ir, Ru and Rh, but to a lesser extent. The onset of magnetite crystallization lowers Fe^{3+} in the melt, which leads to a decline in fO_2 and triggers sulfide saturation (Jenner et al., 2010). This in turn leads to a sharp fall in the concentrations of Cu, Au and PGE, including Pd, in the melt.

The Pual Ridge lavas precipitated a Pt-rich alloy instead of the Ir-rich alloy that is observed in komatiites and Hawaiian picrites and basalts because the Pual Ridge lavas had an appreciably higher Pt/Ir ratio and lower Ir contents than those found in the intra-plate magmas. Our results provide strong evidence that Pt-rich alloys can crystallize from basaltic-andesitic arc-related magmas, along with the silicate minerals, and fractionate Pt from Pd. Given that arc-related lavas commonly have low Ir contents and high Pt/Ir and mafic–ultramafic cumulates from arc environments contain abundant Pt-rich alloys, we suggest that saturation of the Pt-rich alloys may be a common feature of

arc-related magmas. The Pt-rich alloy saturation can be identified from an increase in Pd/Pt with decreasing MgO.

Identifying sulfide saturation in an evolving felsic system is a key to understanding the geochemistry of chalcophile elements and its potential to form magmatic-hydrothermal Cu, Au or Cu–Au ore deposits. The PGE geochemistry, especially a drop in Pd/Cu, can be used to identify sulfide saturation and the formation of an immiscible sulfide melt that sequesters all chalcophile elements including Cu, Au and the PGE, resulting in the observed depletion of Cu and Au at 3 wt.% MgO in the Pual Ridge lavas. The chalcophile elements must be locked in minerals associated with sulfide blebs in a magma chamber below the Pual Ridge. If sulfide saturation occurs before volatile saturation, the roof rocks that overlie such intrusions are not prospective for magmatic hydrothermal Cu, Au or Cu–Au deposits.

ACKNOWLEDGEMENTS

This research was funded by an ARC Discovery Grant to Ian Campbell. The samples used in this study were collected by Dr. Ray Binns of CSIRO during voyages of the RV *Franklin* and RV *Sonne,* which were supported by the Australian Marine National Facility. We would like to thank Charlotte Allen for assistance with the ICP-MS analysis and Graham Mortimer for help in laboratory works at the ANU. We also would like to thank Hugh O'Neill, Frances Jenner, Charlotte Allen, John Mavrogenes and Paolo Sossi for their constructive comments. The present manuscript benefitted greatly from critical comments from Christian Timm, Wolfgang Maier and an anonymous reviewer. Thoughtful comments from Mark Rehkämper greatly enhanced our manuscript.

APPENDIX A. COMPARISON OF PT AND RE DATA WITH PREVIOUS STUDIES

Platinum and Re data from this study are compared with analyses of the same samples taken from the literature (Sun et al., 2003; Jenner et al., 2010) in Fig. A1. The Pual Ridge lavas were analyzed by a Ni–sulfide fire assay – isotope dilution method in this study, and the literature data were obtained by laser ablation inductively coupled plasma mass spectrometry (LA-ICP-MS) (Sun et al., 2003; Jenner et al., 2010). Our Re data are consistent with those from previous studies, although some data from Sun et al. (2003) are anomalously high (>10 ppb) (Fig. A1). The high Re values were attributed to small sulfide grains trapped in glasses (Sun et al., 2003). In contrast, the Pt concentrations from the present study are systematically lower than those from Jenner et al. (2010), especially in the low-Mg lavas, although they show very similar trends in a metal vs. MgO diagram (Fig. A1). This discrepancy may result from sample heterogeneity and/or differences in the analytical methods. Jenner et al. (2010) measured metal concentrations in magmatic glasses by *in situ* LA-ICP-MS whereas we analyzed glass-rich whole-rock samples. As a consequence, the accumulation of PGE-poor silicate phenocrysts could decrease the Pt levels to those found in this study. However, given that Re data in both studies are very similar, this explanation is considered unlikely.

The origin of the difference in Pt data is uncertain. However, it is unlikely that highly evolved silicate melts, such as the Pual ridge low-Mg lavas, contain ~1 ppb of Pt as reported by Jenner et al. (2010), given that the estimated maximum Pt solubility in low-Mg Pual Ridge lavas (0.2 wt.% MgO, 1 mol% H_2O, 1 kbar and fO_2 of QFM + 2) is ~0.3 ppb (Fortenfant et al., 2003). In addition, Jenner et al. (2010) carried out an interference correction on ^{195}Pt to account for isobaric interferences from $^{179}Hf^{16}O$ and $^{155}Gd^{40}Ar$ based on the metal-oxide production rates obtained from analyses of zircon and rutile, which have different matrices to that of a silicate glass. Given that the Pt concentrations of ~1 ppb are close to the detection limit of their LA-ICP-MS analysis (i.e. measured Pt counts are close to background counts), any matrix effect or unrecognized molecular and isobaric interference on ^{195}Pt could greatly affect the calculated Pt concentration. Based on the above discussion, we suggest that the relatively high Pt concentrations in the Pual Ridge lavas reported by Jenner et al. (2010) are an analytical artifact.

REFERENCES

Augé T., Genna A., Legendre O., Ivanov K. S. and Volchenko Y. A. (2005) Primary platinum mineralization in the Nizhny Tagil and Kachkanar Ultramafic complexes, Urals, Russia: A genetic model for PGE concentration in chromite-rich zones. *Econ. Geol.* **100**, 707–732.

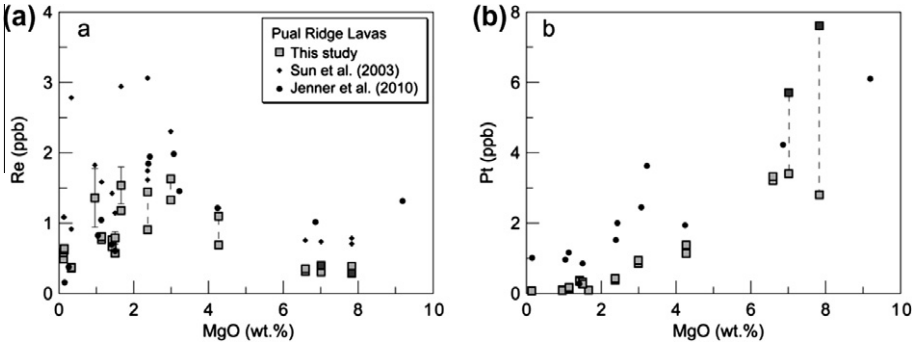

Fig. A1. Comparison of (a) Re and (b) Pt data from the Pual Ridge lavas between this study and previous studies (Sun et al., 2007; Jenner et al., 2010). Two anomalously high Re data (>10 ppb; Sun et al., 2003) are now shown. Note that Re and Pt data in this study are consistently lower than the values reported in the previous studies, especially at low concentration of Pt. Black squares represent phenocryst-bearing samples.

Appendix B
PGE and Re concentrations measured by Agilent 7500 and Agilent 7700x ICP-MS.

Sample	Re		Pd		Pt		Rh		Ru		Ir	
MD3[a]	0.35	±0.03	7.53	±0.22	2.82	±0.12	0.185	±0.008	0.289	±0.035	0.069	±0.003
MD3[b]	0.41	±0.02	7.69	±0.10	2.77	±0.07	0.189	±0.008	0.287	±0.008	0.071	±0.004
MD3-p[a]	0.29	±0.03	10.44	±0.30	7.73	±0.32	0.376	±0.017	0.648	±0.077	0.152	±0.006
MD3-p[b]	0.28	±0.04	10.42	±0.31	7.50	±0.13	0.394	±0.015	0.629	±0.049	0.141	±0.007
86DR[a]	1.01	±0.05	20.80	±0.56	1.36	±0.12	0.126	±0.006	*0.007*	*±0.002*		
86DR[b]	1.18	±0.19	21.18	±0.41	1.37	±0.04	0.126	±0.006	0.011	±0.004	0.0043	±0.0003
MD7[a]	1.53	±0.63	2.08	±0.03	0.95	±0.10						
MD7[b]	1.72	±0.12	2.15	±0.05	0.90	±0.03	0.0059	±0.0012	*0.0028*	*±0.0018*	0.0012	±0.0004
MD53A[a]	1.58	±0.04	1.42	±0.03	0.41	±0.03	0.031	±0.001			0.024	±0.004
MD53A[b]	1.30	±0.07	1.39	±0.04	0.41	±0.02	0.029	±0.001	0.0072	±0.0013	0.022	±0.001
MD53B[a]	1.23	±0.08	0.18	±0.01	0.084	±0.023	0.0025	±0.0008	<0.0026			
MD53B[b]	1.12	±0.05	0.17	±0.01	<0.052		0.0028	±0.0005	<0.0026		<0.0008	
MD36[a]			0.041	±0.012	0.080	±0.019						
MD36[b]			0.044	±0.006	0.070	±0.018	0.0027	±0.0007	<0.0026		<0.0008	
MD28[a]	0.72	±0.10	0.67	±0.04	0.34	±0.03	0.020	±0.003	0.014	±0.009	0.0074	±0.0028
MD28[b]	0.80	±0.02	0.67	±0.01	0.32	±0.02	0.020	±0.002	0.013	±0.002	0.0070	±0.0006
MD65[a]	0.60	±0.06	0.73	±0.03	0.25	±0.02	0.020	±0.002	0.011	±0.009	0.0052	±0.0016
MD65[b]	0.53	±0.03	0.75	±0.01	0.26	±0.02	0.021	±0.002	0.014	±0.002	0.0067	±0.0009
MD114[a]	0.89	±0.06	0.14	±0.01	0.17	±0.02	0.0061	±0.0010			0.0090	±0.0012
MD114[b]	0.72	±0.02	0.14	±0.01	0.15	±0.02	0.0064	±0.0006	0.0025	±0.0017	0.010	±0.001
MD39[a]	0.61	±0.18	<0.015		<0.052		0.0031	±0.0013				
MD39[b]	0.54	±0.02	<0.015		<0.052		0.0044	±0.0009	<0.0026		<0.0008	
MD6[a]	0.65	±0.25	0.052	±0.013	0.060	±0.032						
MD6[b]	0.62	±0.04	0.042	±0.010	<0.052		0.0054	±0.0015	0.0040	±0.0027	0.0015	±0.0004
87DR[a]	0.37	±0.10	<0.015		<0.052		0.0018	±0.0009	<0.0026		<0.0008	
87DR[b]	0.36	±0.02	<0.015		<0.052		0.0025	±0.0006	<0.0026		<0.0008	

Note: The data presented here were measured by both Agilent 7500 and 7700x using the same sample solution. The average data are presented in Table 1. Ruthenium data with high interference corrections (>50%) are indicated in italic. Analytical uncertainties are quoted at 1σ.

[a] Obtained using Agilent 7500.

[b] Obtained using Agilent 7700x.

Ballhaus C., Ryan C. G., Mernagh T. P. and Green D. H. (1994) The partitioning of Fe, Ni, Cu, Pt, and Au between sulfide, metal, and fluid phases – a pilot-study. *Geochim. Cosmochim. Acta* **58**, 811–826.

Barnes S.-J., Boyd R., Korneliussen L.-P., Nilsson L.-P., Often M., Pedersen R. B. and Robins B. (1988) The use of mantle normalization and metal ratios in discriminating between the effect of partial melting, crystal fractionation and sulphide segregation on platinum-group elements, gold, nickel and copper: examples from Norway. In *Geo-Platinum 87* (eds. H. Prichard, P. J. Potts, J. F. W. Bowles and S. J. Cribb). Elsevier, Barking, UK, pp. 113–143.

Barnes S.-J., Naldrett A. J. and Gorton M. P. (1985) The origin of the fractionation of platinum-group elements in terrestrial magmas. *Chem. Geol.* **53**, 303–323.

Barnes S. J. and Fiorentini M. L. (2008) Iridium, ruthenium and rhodium in komatiites: evidence for iridium alloy saturation. *Chem. Geol.* **257**, 44–58.

Bezmen N. I., Asif M., Brügmann G. E., Romanenko I. M. and Naldrett A. J. (1994) Distribution of Pd, Rh, Ru, Jr, Os, and Au between sulfide and silicate metals. *Geochim. Cosmochim. Acta* **58**, 1251–1260.

Bezos A., Lorand J. P., Humler E. and Gros M. (2005) Platinum-group element systematics in mid-oceanic ridge basaltic glasses from the Pacific, Atlantic, and Indian Oceans. *Geochim. Cosmochim. Acta* **69**, 2613–2627.

Borisov A. and Palme H. (1997) Experimental determination of the solubility of platinum in silicate melts. *Geochim. Cosmochim. Acta* **61**, 4349–4357.

Borisov A. and Palme H. (2000) Solubilities of noble metals in Fe-containing silicate melts as derived from experiments in Fe-free systems. *Am. Mineral.* **85**, 1665–1673.

Brenan J. M. and Andrews D. (2001) High-temperature stability of laurite and Ru–Os–Ir alloy and their role in PGE fractionation in mafic magmas. *Can. Mineral.* **39**, 341–360.

Brenan J. M., Finnigan C. F., McDonough W. F. and Homolova V. (2012) Experimental constraints on the partitioning of Ru, Rh, Ir, Pt and Pd between chromite and silicate melt: the importance of ferric iron. *Chem. Geol.* **302**, 16–32.

Brenan J. M., McDonough W. F. and Ash R. (2005) An experimental study of the solubility and partitioning of iridium, osmium and gold between olivine and silicate melt. *Earth Planet. Sci. Lett.* **237**, 855–872.

Brenan J. M., McDonough W. F. and Dalpe C. (2003) Experimental constraints on the partitioning of rhenium and some platinum-group elements between olivine and silicate melt. *Earth Planet. Sci. Lett.* **212**, 135–150.

Brügmann G. E., Arndt N. T., Hofmann A. W. and Tobschall H. J. (1987) Noble-metal abundances in komatiite suites from Alexo, Ontario, and Gorgona-Island, Colombia. *Geochim. Cosmochim. Acta* **51**, 2159–2169.

Brügmann G. E., Naldrett A. J., Asif M., Lightfoot P. C., Gorbachev N. S. and Fedorenko V. A. (1993) Siderophile and chalcophile metals as tracers of the evolution of the Siberian Trap in the Noril'sk region, Russia. *Geochim. Cosmochim. Acta* **57**, 2001–2018.

Campbell I. H. and Barnes S. J. (1984) A model for the geochemistry of the platinum-group elements in magmatic sulfide deposits. *Can. Mineral.* **22**, 151–160.

Campbell I. H. and Naldrett A. J. (1979) Influence of silicate – sulfide ratios on the geochemistry of magmatic sulfides. *Econ. Geol.* **74**, 1503–1506.

Capobianco C. J. and Drake M. J. (1990) Partitioning of ruthenium, rhodium, and palladium between spinel and silicate melt and implications for platinum group element fractionation trends. *Geochim. Cosmochim. Acta* **54**, 869–874.

Capobianco C. J. and Drake M. J. (1994) Partitioning and solubility of PGEs in oxides and silicates. *Mineral. Mag.* **58A**, 144–145.

Capobianco C. J., Hervig R. L. and Drake M. J. (1994) Experiments on crystal liquid partitioning of Ru, Rh and Pd for magnetite and hematite solid-solutions crystallized from silicate melt. *Chem. Geol.* **113**, 23–43.

Chazey W. J. and Neal C. R. (2005) Platinum-group element constraints on source composition and magma evolution of the Kerguelen Plateau using basalts from ODP Leg 183. *Geochim. Cosmochim. Acta* **69**, 4685–4701.

Crocket J. H. (2000) PGE in fresh basalt, hydrothermal alteration products, and volcanic incrustations of Kilauea volcano, Hawaii. *Geochim. Cosmochim. Acta* **64**, 1791–1807.

Crocket J. H., Fleet M. E. and Stone W. E. (1997) Implications of composition for experimental partitioning of platinum-group elements and gold between sulfide liquid and basalt melt: the significance of nickel content. *Geochim. Cosmochim. Acta* **61**, 4139–4149.

Dale C. W., Burton K. W., Pearson D. G., Gannoun A., Alard O., Argles T. W. and Parkinson I. J. (2009) Highly siderophile element behaviour accompanying subduction of oceanic crust: whole rock and mineral-scale insights from a high-pressure terrain. *Geochim. Cosmochim. Acta* **73**, 1394–1416.

Dale C. W., Macpherson C. G., Pearson D. G., Hammond S. J. and Arculus R. J. (2012) Inter-element fractionation of highly siderophile elements in the Tonga Arc due to flux melting of a depleted source. *Geochim. Cosmochim. Acta* **89**, 202–225.

Ertel W., O'Neill H. S., Sylvester P. J. and Dingwell D. B. (1999) Solubilities of Pt and Rh in a haplobasaltic silicate melt at 1300 °C. *Geochim. Cosmochim. Acta* **63**, 2439–2449.

Evans N. J., Davis J. J., Byrne J. P. and French D. (2003) Contamination-free preparation of geological samples for ultra-trace gold and platinum-group element analysis. *J. Geochem. Explor.* **80**, 19–24.

Ewart A. and Griffin W. L. (1994) Application of proton-microprobe data to trace-element partitioning in volcanic-rocks. *Chem. Geol.* **117**, 251–284.

Fleet M. E., Crocket J. H., Liu M. H. and Stone W. E. (1999) Laboratory partitioning of platinum-group elements (PGE) and gold with application to magmatic sulfide-PGE deposits. *Lithos* **47**, 127–142.

Fleet M. E. and Wu T. W. (1993) Volatile transport of platinum-group elements in sulfide-chloride assemblages at 1000 °C. *Geochim. Cosmochim. Acta* **57**, 3519–3531.

Fleet M. E. and Wu T. W. (1995) Volatile transport of precious metals at 1000 °C – speciation, fractionation, and effect of base-metal sulfide. *Geochim. Cosmochim. Acta* **59**, 487–495.

Fonseca R. O. C., Campbell I. H., O'Neill H. S. C. and Allen C. M. (2009) Solubility of Pt in sulphide mattes: implications for the genesis of PGE-rich horizons in layered intrusions. *Geochim. Cosmochim. Acta* **73**, 5764–5777.

Fonseca R. O. C., Mallmann G., O'Neill H. S. C. and Campbell I. H. (2007) How chalcophile is rhenium? An experimental study of the solubility of Re in sulphide mattes. *Earth Planet. Sci. Lett.* **260**, 537–548.

Fortenfant S. S., Gunther D., Dingwell D. B. and Rubie D. C. (2003) Temperature dependence of Pt and Rh solubilities in a haplobasaltic melt. *Geochim. Cosmochim. Acta* **67**, 123–131.

Francis R. D. (1990) Sulfide globules in midocean ridge basalts (MORB), and the effect of oxygen abundance in Fe–S–O liquids on the ability of those liquids to partition metals from Morb and Komatiite Magmas. *Chem. Geol.* **85**, 199–213.

Fujimaki H. (1986) Partition-coefficients of Hf, Zr, and REE between Zircon, Apatite, and Liquid. *Contrib. Mineral. Petrol.* **94**, 42–45.

Garuti G., Pushkarev E. V. and Zaccarini F. (2002) Composition and paragenesis of Pt alloys from chromitites of the Uralian-Alaskan-type Kytlym and Uktus complexes, northern and central Urals, Russia. *Can. Mineral.* **40**, 357–376.

Garuti G., Pushkarev E. V., Zaccarini F., Cabella R. and Anikina E. (2003) Chromite composition and platinum-group mineral assemblage in the Uktus Uralian-Alaskan-type complex (Central Urals, Russia). *Miner. Deposita* **38**, 312–326.

Gill J. B. (1981) *Orogenic andesites and plate tectonics*. Springer, Berlin.

Govindaraju K. (1994) Compilation of working values and sample description for 383 Geostandards (vol. 18, p. 53, 1994). *Geostandards Newsletter* **18**, 331–334.

Greenough, J. D. and Fryer, B. J. (1990) Distribution of gold, palladium, platinum, rhodium, ruthenium, and iridium in Leg 115 hotspot basalts: implications for magmatic processes. In *Proceedings of Scientific Results, ODP, Leg 115*. Mascarene, Plateau, pp. 71–84.

Hanley J. J. and Heinrich C. A. (2007) Synthetic melt inclusion and quartz-trap methods for determining Pt solubility in a mafic mineral – Halide melt system at 750 °C, 400 bar. *Geochim. Cosmochim. Acta* **71**, A378.

Hanley J. J., Pettke T., Mungall J. E. and Spooner E. T. C. (2005) The solubility of platinum and gold in NaCl brines at 1.5 kbar, 600–800 °C: A laser ablation ICP-MS pilot study of synthetic fluid inclusions. *Geochim. Cosmochim. Acta* **69**, 2593–2611.

Hill E., Wood B. J. and Blundy J. D. (2000) The effect of Ca-Tschermaks component on trace element partitioning between clinopyroxene and silicate melt. *Lithos* **53**, 203–215.

Ireland T. J., Walker R. J. and Garcia M. O. (2009) Highly siderophile element and Os isotope systematics of Hawaiian picrites: implications for parental melt composition and source heterogeneity. *Chem. Geol.* **260**, 112–128.

Jamais M., Lassiter J. C. and Brügmann G. (2008) PGE and Os-isotopic variations in lavas from Kohala Volcano, Hawaii: constraints on PGE behavior and melt/crust interaction. *Chem. Geol.* **250**, 16–28.

Jenner F. E., O'Neill H. S. C., Arculus R. J. and Mavrogenes J. A. (2010) The magnetite crisis in the evolution of arc-related magmas and the initial concentration of Au, Ag and Cu. *J. Petrol.* **51**, 2445–2464.

Kamenetsky V. S., Binns R. A., Gemmell J. B., Crawford A. J., Mernagh T. P., Maas R. and Steele D. (2001) Parental basaltic melts and fluids in eastern Manus backarc Basin: implications for hydrothermal mineralisation. *Earth Planet. Sci. Lett.* **184**, 685–702.

Keays R. R. and Campbell I. H. (1981) Precious metals in the Jimberlana Intrusion, Western-Australia - implications for the genesis of platiniferous ores in layered intrusions. *Econ. Geol.* **76**, 1118–1141.

Kepezhinskas P., Defant M. J. and Widom E. (2002) Abundance and distribution of PGE and Au in the island-arc mantle: implications for sub-arc metasomatism. *Lithos* **60**, 113–128.

Lorand J. P., Alard O. and Luguet A. (2010) Platinum-group element micronuggets and refertilization process in Lherz orogenic peridotite (northeastern Pyrenees, France). *Earth Planet. Sci. Lett.* **289**, 298–310.

Lorand J. P., Luguet A., Alard O., Bezos A. and Meisel T. (2008) Abundance and distribution of platinum-group elements in

orogenic lherzolites; a case study in a Fontete Rouge lherzolite (French Pyrenees). *Chem. Geol.* **248**, 174–194.

Lorand J. P., Pattou L. and Gros M. (1999) Fractionation of platinum-group elements and gold in the upper mantle: a detailed study in Pyrenean orogenic lherzolites. *J. Petrol.* **40**, 957–981.

Maier W. D. and Barnes S.-J. (2004) Pt/Pd and Pd/Ir ratios in mantle-derived magmas: a possible role for mantle metasomatism. *South Afr. J. Geol.* **107**, 333–340.

Mallmann G. and O'Neill H. S. C. (2007) The effect of oxygen fugacity on the partitioning of Re between crystals and silicate melt during mantle melting. *Geochim. Cosmochim. Acta* **71**, 2837–2857.

Martinez F. and Taylor B. (1996) Backarc spreading, rifting, and microplate rotation, between transform faults in the Manus basin. *Mar. Geophys. Res.* **18**, 203–224.

McDonough W. F. and Sun S. S. (1995) The composition of the Earth. *Chem. Geol.* **120**, 223–253.

McInnes B. I. A., McBride J. S., Evans N. J., Lambert D. D. and Andrew A. S. (1999) Osmium isotope constraints on ore metal recycling in subduction zones. *Science* **286**, 512–516.

Meisel T., Fellner N. and Moser J. (2003) A simple procedure for the determination of platinum group elements and rhenium (Ru, Rh, Pd, Re, Os Ir and Pt) using ID-ICP-MS with an inexpensive on-line matrix separation in geological and environmental materials (vol. 18, p. 720, 2003). *J. Anal. Atom Spectrom.* **18**, 1318.

Meisel T. and Moser J. (2004) Platinum-group element and rhenium concentrations in low abundance reference materials. *Geostand. Geoanal. Res.* **28**, 233–250.

Momme P., Tegner C., Brooks C. K. and Keays R. R. (2002) The behaviour of platinum-group elements in basalts from the East Greenland rifted margin. *Contrib. Mineral. Petrol.* **143**, 133–153.

Moss R., Scott S. D. and Binns R. A. (2001) Gold content of Eastern Manus Basin volcanic rocks: implications for enrichment in associated hydrothermal precipitates. *Econ. Geol. Bull. Soc.* **96**, 91–107.

Mungall J. E., Karrei L. I., Arculus R. J. and Mavrogenes J. A. (2011) *Controls on platinum-group element abundances in 110 samples of arc lavas from the Southwest Pacific*. AGU Fall Meeting San Francisco, California.

Park J.-W., Campbell I. H. and Eggins S. M. (2012a) Enrichment of Rh, Ru, Ir and Os in Cr spinels from oxidized magmas: evidence from the Ambae volcano. *Vanuatu. Geochim. Cosmochim. Acta* **78**, 28–50.

Park J.-W., Campbell I. H., Ickert R. B. and Allen C. M. (2012b) Chalcophile element geochemistry of the Boggy Plain Zoned Pluton, southeastern Australia: A S-saturated barren compositionally diverse magma. Contrib. Mineral. Petrol. http://dx.doi.org/10.1007/s00410-012-0806-9.

Park J.-W., Hu Z., Gao S., Campbell I. H. and Gong H. (2012c) Platinum group element abundances in the upper continental crust revisited - New constraints from analyses of Chinese loess. *Geochim. Cosmochim. Acta* **93**, 63–76.

Park S. H., Lee S. M., Kamenov G. D., Kwon S. T. and Lee K. Y. (2010) Tracing the origin of subduction components beneath the South East rift in the Manus Basin, Papua New Guinea. *Chem. Geol.* **269**, 339–349.

Peach C. L., Mathez E. A. and Keays R. R. (1990) Sulfide melt-silicate melt distribution coefficients for noble metals and other chalcophile elements as deduced from MORB: implications for partial melting. *Geochim. Cosmochim. Acta* **54**, 3379–3389.

Peck D. C., Keays R. R. and Ford R. J. (1992) Direct crystallization of refractory platinum-group element alloys from boninitic magmas – evidence from Western Tasmania. *Aust. J. Earth Sci.* **39**, 373–387.

Peucker-Ehrenbrink, B., Bach, W., Hart, S.R., Blusztajn, J. S. and Abbruzzese, T. (2003) Rhenium-osmium isotope systematics and platinum group element concentrations in oceanic crust from DSDP/ODP Sites 504 and 417/418. *Geochem. Geophys. Geosytm.* **4**.

Philipp H., Eckhardt J. D. and Puchelt H. (2001) Platinum-group elements (PGE) in basalts of the seaward-dipping reflector sequence, SE Greenland coast. *J. Petrol.* **42**, 407–432.

Pitcher L., Helz R. T., Walker R. J. and Piccoli P. (2009) Fractionation of the platinum-group elements and Re during crystallization of basalt in Kilauea Iki Lava Lake, Hawaii. *Chem. Geol.* **260**, 196–210.

Pruseth K. L. and Palme H. (2004) The solubility of Pt in liquid Fe-sulfides. *Chem. Geol.* **208**, 233–245.

Puchtel I. S. and Humayun M. (2001) Platinum group element fractionation in a komatiitic basalt lava lake. *Geochim. Cosmochim. Acta* **65**, 2979–2993.

Puchtel I. S., Humayun M., Campbell A. J., Sproule R. A. and Lesher C. M. (2004) Platinum group element geochemistry of komatiites from the Alexo and Pyke Hill areas, Ontario, Canada. *Geochim. Cosmochim. Acta* **68**, 1361–1383.

Rehkämper M., Halliday A. N., Barfod D. and Fitton J. G. (1997) Platinum-group element abundance patterns in different mantle environments. *Science* **278**, 1595–1598.

Rehkämper M., Halliday A. N., Fitton J. G., Lee D. C., Wieneke M. and Arndt N. T. (1999) Ir, Ru, Pt, and Pd in basalts and komatiites: new constraints for the geochemical behavior of the platinum-group elements in the mantle. *Geochim. Cosmochim. Acta* **63**, 3915–3934.

Righter K., Campbell A. J., Humayun M. and Hervig R. L. (2004) Partitioning of Ru, Rh, Pd, Re, Ir, and Au between Cr-bearing spinel, olivine, pyroxene and silicate melts. *Geochim. Cosmochim. Acta* **68**, 867–880.

Righter K., Chesley J. T., Geist D. and Ruiz J. (1998) Behavior of Re during magma fractionation: an example from Volcan Alcedo, Galapagos. *J. Petrol.* **39**, 785–795.

Ripley E. M., Brophy J. G. and Li C. S. (2002) Copper solubility in a basaltic melt and sulfide liquid/silicate melt partition coefficients of Cu and Fe. *Geochim. Cosmochim. Acta* **66**, 2791–2800.

Robb L. J. (2004) *Introduction to Ore-forming Processes*. Blackwell Publishing, Oxford.

Savard D., Barnes S.-J. and Meisel T. (2010) Comparison between nickel–sulfur fire assay te co-precipitation and isotope dilution with high-pressure asher acid digestion for the determination of platinum-group elements, rhenium and gold. *Geostand. Geoanal. Res.* **34**, 281–291.

Simon A. C. and Pettke T. (2009) Platinum solubility and partitioning in a felsic melt-vapor-brine assemblage. *Geochim. Cosmochim. Acta* **73**, 438–454.

Simon A. C., Pettke T., Candela P. A., Piccolli P. M. and Heinrich C. A. (2006) Copper partitioning in a melt-vapor-brine-magnetite-pyrrhotite assemblage. *Geochim. Cosmochim. Acta* **70**, 5583–5600.

Sinton J. M., Ford L. L., Chappell B. and Mcculloch M. T. (2003) Magma genesis and mantle heterogeneity in the Manus back-arc basin, Papua New Guinea. *J. Petrol.* **44**, 159–195.

Song X. Y., Keays R. R., Xiao L., Qi H. W. and Ihlenfeld C. (2009) Platinum-group element geochemistry of the continental flood basalts in the central Emeisihan Large Igneous Province, SW China. *Chem. Geol.* **262**, 246–261.

Spandler C. J., Arculus R. J., Eggins S. M., Mavrogenes J. A., Price R. C. and Reay A. J. (2003) Petrogenesis of the Greenhills complex, southland, New Zealand: Magmatic differentiation

and cumulate formation at the roots of a Permian island-arc volcano. *Contrib. Mineral. Petrol.* **144**, 703–721.

Spandler C. J., Eggins S. M., Arculus R. J. and Mavrogenes J. A. (2000) Using melt inclusions to determine parent-magma compositionsof layered intrusions: application to the Greenhills Complex (New Zealand), a platinum group minerals-bearing, island-arcintrusion. *Geology* **28**, 991–994.

Sugawara T. (2000) Empirical relationships between temperature, pressure, and MgO content in olivine and pyroxene saturated liquid. *J. Geophys. Res.-Sol. Ea* **105**, 8457–8472.

Sun W. D., Arculus R. J., Bennett V. C., Eggins S. M. and Binns R. A. (2003) Evidence for rhenium enrichment in the mantle wedge from submarine arc-like volcanic glasses (Papua New Guinea). *Geology* **31**, 845–848.

Sun W. D., Arculus R. J., Kamenetsky V. S. and Binns R. A. (2004) Release of gold-bearing fluids in convergent margin magmas prompted by magnetite crystallization. *Nature* **431**, 975–978.

Sun W. D., Binns R. A., Fan A. C., Kamenetsky V. S., Wysoczanski R., Wei G. J., Hu Y. H. and Arculus R. J. (2007) Chlorine in submarine volcanic glasses from the Eastern Manus Basin. *Geochim. Cosmochim. Acta* **71**, 1542–1552.

Taylor B., Crook K. and Sinton J. (1994) Extensional transform zones and oblique spreading centers. *J. Geophys. Res.-Sol. Ea* **99**, 19707–19718.

Vogel D. C. and Keays R. R. (1997) The petrogenesis and platinum-group element geochemistry of the Newer Volcanic Province, Victoria, Australia. *Chem. Geol.* **136**, 181–204.

Williams T. J., Candela P. A. and Piccoli P. M. (1995) The partitioning of copper between silicate melts and two-phase aqueous fluids: an experimental investigation at 1 kbar, 800 °C and 0.5 kbar, 850 °C. *Contrib. Mineral. Petrol.* **121**, 388–399.

Wood S. A. (1987) Thermodynamic calculations of the volatility of the platinum group elements (Pge) – the Pge content of fluids at magmatic temperatures. *Geochim. Cosmochim. Acta* **51**, 3041–3050.

Woodland S. J., Pearson D. G. and Thirlwall M. F. (2002) A platinum group element and Re-Os isotope investigation of siderophile element recycling in subduction zones: comparison of Grenada, Lesser Antilles arc, and the Izu-Bonin arc. *J. Petrol.* **43**, 171–198.

Zaccarini F., Garuti G. and Pushkarev E. V. (2011) Unusually pge-rich chromitite in the butyrin vein of the Kytlym Uralian-Alaskan complex, northern urals, Russia. *Can. Mineral.* **49**, 1413–1431.

Associate editor: Mark Rehkamper